THE ASTROPHYSICAL JOURNAL, 510:379–403, 1999 January 1
© 1999. The American Astronomical Society. All rights reserved. Printed in U.S.A.

THE EXPULSION OF STELLAR ENVELOPES IN CORE-COLLAPSE SUPERNOVAE

CHRISTOPHER D. MATZNER AND CHRISTOPHER F. MCKEE
Departments of Physics and Astronomy, 601 Campbell Hall, University of California, Berkeley, Berkeley, CA 94720; matzner@astron.berkeley.edu, cmckee@mckee.berkeley.edu
Received 1998 May 5; accepted 1998 August 4

ABSTRACT

We examine the relation between presupernova stellar structure and the distribution of ejecta in core-collapse supernovae of Types Ib, Ic, and II, under the approximations of adiabatic, spherically symmetric flow. We develop a simple yet accurate analytical formula for the velocity of the initial forward shock that traverses the stellar envelope. For material that does not later experience a strong reverse shock, the entropy deposited by this forward shock persists into the final, freely expanding state. We demonstrate that the final density distribution can be approximated with simple models for the final pressure distribution, in a way that matches the results of simulations. Our results indicate that the distribution of density and radiation pressure in a star's ejecta depends on whether the outer envelope is radiative or convective, and if convective, on the composition structure of the star. Our models are most accurate for the high-velocity ejecta cast away from the periphery of a star. For stellar structures that limit to a common form in this region, the resulting ejecta limit to a common distribution at high velocities because the blast wave forgets its history as it approaches the stellar surface. We present formulae for the final density distribution of this material as a function of mass, for both radiative and efficiently convective envelopes. These formulae limit to the well-known planar, self-similar solutions for mass shells approaching the stellar surface. However, the assumption of adiabatic flow breaks down for shells of low optical depth, so this planar limit need not be attained. The event of shock emergence, which limits adiabatic flow, also produces a soft X-ray burst of radiation. Formulae are given for the observable properties of this burst and their dependence on the parameters of the explosion. Motivated by the relativistic expansion recently inferred by Kulkarni et al. for the synchrotron shell around SN 1998bw, we estimate the criterion for relativistic mass ejection and the rest mass of relativistic ejecta. We base our models for the entire ejecta distribution on the high-velocity solution, on our shock-velocity formula, and on realistic radiation pressure distributions. We also present simpler, but less flexible, analytical approximations for ejecta distributions. We survey the ejecta of the polytropic hydrogen envelopes of red supergiants. Our models will be useful for studies of the light curves and circumstellar or interstellar interactions of core-collapse supernovae, and of the birth of pulsar nebulae in their ejecta.

Subject headings: hydrodynamics — shock waves — stars: interiors — supernova remnants — supernovae: general — supernovae: individual (SN 1987A)

1. INTRODUCTION

All stars of initial mass greater than about $8M_\odot$ end violently when their cores collapse; many or all of these produce supernova explosions. Supernovae are of paramount importance to the evolution of galaxies: they form new elements and recycle the products of stellar evolution. Their energy is converted into motion and heat, affecting the dynamical state of the surrounding gas; indeed, they are responsible for much of the hot, X-ray–emitting gas in galaxies and for the formation of superbubbles and outflow in starburst galaxies. Observationally, supernovae provide a natural laboratory in which to test theories of stellar evolution and of the circumstellar environments of massive stars: SN 1987A is a notable example (McCray 1993).

How does the stellar structure of a progenitor affect the aftermath of its explosion? The observable properties of a core-collapse supernova are determined by the distribution of material and temperature in its freely expanding ejecta. The supernova's optical display begins with a photospheric stage, in which a recombination front moves inward through the expanding ejecta. This process is predetermined by the temperature, density, and opacity profiles of the outcast material. At some point, the energy from radioactive decays begins to dominate the light curve. The nebular display is determined by the distributions of both decaying isotopes and gamma-ray opacity. Later, as the ejecta collide with circumstellar or interstellar material, two shocks are born at the interface: a forward shock accelerating the surrounding material and a reverse shock decelerating the ejecta (McKee 1974; Chevalier 1982; Dwarkadas & Chevalier 1998; Truelove & McKee 1998). This interaction depends critically on the distributions of ejected and ambient material. It is responsible for the appearance of the supernova in the radio, X-ray, and infrared bands for centuries after the explosion.

The distributions that characterize a supernova's ejecta are, in turn, determined uniquely by the structure of the progenitor star (although the distribution of radioactive elements is an added complication). The relation between progenitor and ejecta is established by the hydrodynamics of the supernova explosion itself, which occurs in three stages. In the first stage, a shock propagates through the stellar material to be ejected, pressurizing it and setting it into motion: we call this the "blastwave" stage, following Chevalier (1976). Once the shock arrives at the stellar surface, a "rarefaction" phase begins: the material accelerates as its heat is converted into kinetic energy. This stage (the most difficult to model) ends when acceleration ceases, once the ejecta's pressure is too slight to be dynamically important. In the "ejecta" stage, the outcast material coasts into

homologous expansion, with a velocity distribution $v = r/t$.

The correspondence between progenitor and ejecta can be established numerically on a case-by-case basis. This approach has been pursued for many years (see, e.g., Falk & Arnett 1977). However, many aspects of the late stages of stellar evolution are uncertain, including rotation and pulsations (Heger et al. 1997), nuclear reaction rates, mass-loss prescriptions, and models for semiconvection (Woosley, Langer, & Weaver 1993), and it is likely that interactions with stellar (see, e.g., Nomoto, Iwamoto, & Suzuki 1995) or substellar companions will affect supernova progenitors. Numerical simulations may describe specific cases quite accurately, but only limited insight into the physical relationship between progenitor and ejecta can be derived from an individual case.

Supernova progenitors and their ejecta display strikingly similar features when the initial and final densities are considered functions of a Lagrangian variable, like the enclosed mass. Does this imply that there is a simple relationship between the two? This paper will investigate the existence of such a relationship—that is, the degree to which the variables that describe a mass shell in the progenitor control its properties after the explosion happens. A local relation between the initial and final variables implies that the physics of the explosion can be understood in simple terms, despite the complicated hydrodynamical interactions involved. The pressure-based models of § 6 demonstrate that this is the case.

Another goal of this paper will be to provide simple models for broad classes of supernova progenitors, like red supergiants. When progenitor stars are similar in structure, their ejecta will also take similar distributions. A simple model that can reproduce these ejecta accurately enough to show the differences between them, like the harmonic-mean models of § 7, should prove valuable for studies of supernova light curves and circumstellar interactions.

1.1. *Previous Investigations*

The analytical study of supernova hydrodynamics has relied on familiar self-similar analogs. Over a considerable fraction of the progenitor, the density distribution resembles a power law in radius: $\rho_0 \propto r_0^{-n}$ with $n \sim 1.5$–3 above the core, but usually with a shallower distribution farther out. In a strictly power-law, spherical distribution, the blastwave stage takes the self-similar form given by Taylor (1950) and Sedov (1959). Chevalier (1976) likened the structure of a blastwave in an increasingly steep density distribution to a progression of Sedov blastwaves in different power-law media and concluded that a detached shell (density maximum) would occur if density became steeper than a critical value. By analogy to the Sedov blastwave with $\rho_0 \propto r_0^{-3}$, Bethe & Pizzochero (1990) conjectured that the shock in SN 1987A would have nearly a constant velocity. Chevalier & Soker (1989) approximated the central progenitor distribution as $\rho_0 \propto r_0^{-17/7}$, which produces a particularly simple blastwave distribution (the Primakoff-Sedov form) in which density and pressure are power laws in radius and time.

The resemblance to a Sedov blastwave must break down as the shock approaches and emerges from the stellar surface and the rarefaction phase begins, but there is an analytical solution to guide the understanding of this process as well. The density varies as a power of depth in the outer layers of a star, and radial curvature can be neglected near enough to the stellar surface. A planar version of this problem was initially considered by Gandel'man & Frank-Kamenetsky (1956) and solved by Sakurai (1960). In this context, the shock front accelerates as it runs down the declining density gradient, and material expands into vacuum after the shock emerges from the surface. The ratio of final to postshock velocity is the same for all fluid elements in this solution; the density and pressure approach steep power laws in velocity as the material expands freely. This solution has been applied to the pulse of emission associated with shock breakout and the early phase of the light curve (Chevalier 1992), as well as the distribution of high-velocity ejecta from the explosion (see, e.g., Chevalier & Soker 1989; Imshennik & Nadëzhin 1989; Litvinova & Nadëzhin 1990). Imshennik & Nadëzhin (1989) and Chevalier (1992) showed that spherical curvature should complicate matters, because a mass shell in the planar solution must travel a long way (compared to its initial depth) to reach its final velocity. Kazhdan & Murzina (1992)[1] took the dynamical effect of sphericity into account in a first-order perturbation analysis of Sakurai's solution. In this paper, we will find the correction of the planar solution to higher order by a different method.

Sakurai's planar solution describes the end of shock motion and the beginning of rarefaction, but even with the first-order effect of sphericity accounted for, this solution holds only for the highest velocity ejecta, or for the brief period in which the shock crosses and ejects a thin outer shell. It does not describe how this brief period joins onto the blastwave phase that preceded it and the rarefaction phase that follows it, in which the bulk of the ejecta approaches its final velocity. The rarefaction phase is very complicated in general, even if the blastwave was one of the Sedov forms; rarefaction is therefore a formidable problem.

There is one counterexample. For the special case of the Primakoff blastwave, in which density and sound speed are power laws of radius and time, a rarefaction wave will travel along a power-law trajectory. Chevalier & Soker (1989), using the Primakoff form to approximate the blastwave in SN 1987A, argued that the spherical rarefaction process will be self-similar in this case. Then, the ratio between the final velocity and the velocity at the rarefaction wave should be the same for any mass shell. This simple argument specifies that the density should settle into a shallow power law of velocity, in the inner region of the ejecta. Joining this shallow inner power law with the steep outer power law specified by Sakurai's planar solution, and imposing overall mass and energy conservation, Chevalier & Soker found the velocity of the break between the two behaviors. Although it is based on idealizations of the flow, this model compares admirably with simulations involving blue supergiant progenitors.

1.2. *This Work*

In this paper we address each stage of the expulsion of stellar envelopes in core-collapse supernovae, in order to arrive at a reliable model for the final ejecta distribution that can accommodate possible variations in progenitors' stellar structures. Wherever possible, we make use of scaling relations to simplify the problem. When considering red supergiants, we concentrate primarily on the outermost

[1] We are grateful to the referee, R. Chevalier, for bringing this work to our attention.

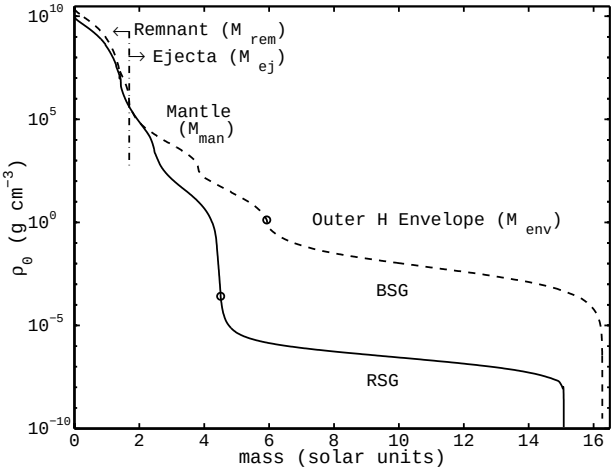

FIG. 1.—Red and blue supergiant progenitors used in this paper. The 15 $M_\odot$ RSG (*solid line*; Woosley & Weaver 1995) was provided by S. Woosley. The 16 $M_\odot$ BSG (*dashed line*; Shigeyama & Nomoto 1990) was provided by K. Nomoto. The boundaries between remnant and ejecta (*dot-dashed line*) and between mantle and outer envelope material (M_α; *circles*) are marked in both cases. We take the remnant to be the edge of the iron core; this gives remnant masses of 1.48 and 1.69 $M_\odot$ for the RSG and BSG, respectively.

composition layer (the hydrogen envelope), where our models will be most accurate, approximating these envelopes as polytropes when it is useful to do so. Table 1 gives an overview of the models developed in this paper; these are motivated by and then checked against simulations for which the initial configuration is the result of a stellar evolution study. These progenitors (see Fig. 1) were kindly supplied to us by S. Woosley and K. Nomoto.

We begin by examining in § 2 the scaling relations that connect the hydrodynamical behavior of similar initial structures, under the idealization of adiabatic flow. The scaling to similar solutions will be especially useful in § 5, where we present solutions for the high-velocity ejecta of convective and radiative envelopes with a single form for each.

Section 3 discusses the general features of supernova progenitor stellar structures. These are marked by composition zones of vastly different density and radial scale. The blastwave shock typically decelerates inside each layer and accelerates in the steep density declines between zones. The shock wave accelerates as it approaches the surface of the star, at the end of the blastwave phase.

The models we develop will require an approximation for the detailed motion of the blastwave shock front. The forward shock defines the outer boundary of the flow in the blastwave stage. Moreover, the blastwave shock velocity sets the entropy distribution for the ensuing adiabatic flow (for material not subject to reverse shocks). The shock velocity thereby affects the rarefaction phase, as well, and the relation between pressure and density in the final ejecta phase. The shock velocity is also necessary to set the coefficients of the power laws that describe the highest velocity ejecta. In reality, the shock velocity must be determined self-consistently by matching it to the postshock pressure in the blastwave phase. Previous studies (Kompaneets 1960; Laumbach & Probstein 1969; Whitham 1974; Klimishin & Gnatyk 1982; Koo & McKee 1990) have suggested a number of formulae for the velocities of shocks in inhomogeneous, three-dimensional distributions; all of these formulae have drawbacks in the context of supernovae, and we will suggest another simple shock velocity formula better adapted to this context in § 4. This shock-velocity approximation is the product of well-known scaling laws for spherical decelerating shocks and planar accelerating shocks. Despite its simplicity, this approximation tracks the successive periods of shock acceleration and deceleration with remarkable accuracy. This approximation gives the entropy distribution in the ejecta, except where a reverse shock interferes. It also gives the coefficients that describe the highest velocity ejecta.

In § 5 we address the dynamics of material near the surface in the progenitor, the material that is ejected at high velocity. The initial distribution of this material, described in § 3.1, has a predictable form in radiative and polytropic envelopes. Having a reliable estimate of the velocity of the shock that launches this material, we calculate in § 5.1 the coefficients of the power laws that describe its ejecta, as given by the planar, self-similar solution (Gandel'man & Frank-Kamenetsky 1956; Sakurai 1960; see the Appendix). Most material attains a smaller velocity than the planar formula would give, because spherical expansion reduces the pressure to below its planar value. This is a geometrical effect, however, and because the initial density distributions of this material are similar among broad classes of envelopes (radiative or convective), the final ejecta distribu-

TABLE 1

MODELS FOR THE EJECTA DENSITY

Parameter	Pressure-based Models (§ 6)	Harmonic-Mean Models (§ 7)
Model output	$\rho_f(m)t^3$	$\rho_f(v)t^3$
Type of model	Local, Lagrangian	Global, Eulerian
Flexibility	Responds to detailed stellar structure	Fixed analytical form
Benefits	Gives jump in ρ_f at mantle	Simple
Drawbacks	Requires initial structure	Insensitive to detailed structure
RSG models[a]	Parameter α fit as $\alpha(q)$	3 parameters fitted with q
	H envelope most accurate	H envelope only
BSG, Ib, Ic models[b]	Approximate $\alpha = 0$	Generalized model of CS89[c]
	Applies to mantle	Approximates mantle

[a] Models for red supergiants are based upon polytropic models for the progenitors; these are primarily determined by one parameter, q.

[b] Radiative progenitors are not easily modeled with simple progenitors, but this is counterbalanced by the fact that features in their ejecta are less pronounced.

[c] "CS89" = Chevalier & Soker 1989.

tions are also similar. In § 5.2, we present simple formulae that capture the deviation of important quantities away from their self-similar power laws.

The self-similar solutions that give power laws for the high-velocity ejecta are not valid to infinite velocity, of course. The assumption of adiabatic flow breaks down for material involved in shock breakout, because radiation diffuses or streams out of the gas. This process also produces a burst of soft X-rays. In § 5.3.1 we present formulae for the upper velocity limit for adiabatic flow. We use our nonrelativistic analysis to derive an approximate criterion for relativistic mass ejection and the rest mass of relativistic ejecta (if any) in § 5.3.2. In § 5.3.3, we present formulae for the characteristics of the X-ray burst. Although previous authors have treated the radiation outburst in a similar manner (see, e.g., Imshennik & Nadëzhin 1989), the shock-velocity formula of § 4 allows us to elucidate the effects of stellar structure on the outburst.

The results of § 5 apply to the high-velocity ejecta, those at velocities a few times greater than the systemic velocity. However, little of the mass or energy in the ejecta lies in this velocity range. For the bulk of ejecta, the details of the progenitor's structure break the scaling relations that allow the high-velocity ejecta to be given accurately by simple formulae. We note that the final pressure distribution is always smooth and continuous in the ejecta, even if the density distribution is not. For this reason, we base our models for the entire ejecta distribution, discussed in § 6, on models for the pressure distribution that mimic the smooth pressure functions seen in simulations. We find a simple way to extend the pressure distributions derived in § 5.2 inward in mass. The final density distribution is specified by the combination of this pressure model with the entropy left behind in the shock. These pressure-based models constitute a local theory, in that they relate the final density of a mass shell with its initial state. These models fail in regions that are traversed by a strong reverse shock, because we do not account for the entropy it deposits; this failure is worst in the inner composition layers of red supergiants. Even so, there is a jump in density between the ejected helium mantle and the ejected hydrogen envelope that is not affected by the reverse shock; a simple analysis of this phenomenon is presented in § 6.1.

Section 7 presents a different type of model for ejecta distributions, in which the shape of the final density is described as a simple, harmonic-mean interpolation between two power laws of velocity. This is a global model, since it gives an ejecta distribution (in terms of three free parameters) without referring to the detailed structure of the progenitor. For blue supergiants, we adopt the theory of Chevalier & Soker (1989) to motivate the choice of parameters. For red supergiants, we find that the harmonic-mean model can fit the ejected hydrogen quite accurately, but it does not fit the ejected mantle because of the density jump between the two regions.

In § 8 we develop simplified polytropic models for red supergiant progenitors of Type II supernovae. We argue that these can be adequately described by two parameters that are ratios of masses in the progenitor. Moreover, these mass ratios are tightly correlated, so that there is essentially a one-parameter family of red supergiant progenitors. We investigate this family of models numerically to find the distribution of the free parameter used in the pressure-based model of § 6 and the three free parameters in the harmonic-mean models of § 7; results are given in Table 4.

Section 9 contains a comparison between our models and the ejecta of simulated supernovae whose progenitors are the end products of stellar evolution calculations. This comparison allows a tabulation of the errors introduced in the pressure-based and harmonic-mean models (Table 6) in a realistic context. The models developed in this paper help to explain many of the features seen in numerical simulations of supernovae. This is true even for features that are not reproduced accurately by the models, those caused by reverse shocks or by variations in the polytropic index at the outside of the progenitor. These features are discussed in § 9 and in the Conclusions.

In the Appendix, we develop a fully Lagrangian treatment of the self-similar shock acceleration problem solved by Sakurai. This problem has previously been addressed in two steps, with a Eulerian solution prior to emergence matched to a Lagrangian description of the subsequent expansion. The fully Lagrangian description facilitates analyses of the highest velocity material. We use it to compare our results from § 5.2 to the suggestion of Litvinova & Nadëzhin (1990) that spherical expansion essentially truncates planar, self-similar acceleration, and we find that this happens at about 3 stellar radii.

2. SCALING TO SIMILAR SOLUTIONS

Although the phenomenon of core collapse is quite complex (see, e.g., Colgate 1995), the resulting blastwave in the stellar envelope has relatively simple dynamics. Gravity is relatively insignificant except for the interior layers, which may suffer infall. The gain or loss of energy to nuclear reactions is also dynamically insignificant except for these inner layers, although they are probably mixed to higher velocities by the Rayleigh-Taylor instability. (Heat from decaying ^{56}Ni may blow bubbles in the ejecta; Arnett, Fryxell, & Müller 1989; Li, McCray, & Sunyaev 1993). Likewise, neutrino heating is negligible outside the dense circumnuclear material. The pressure is radiation dominated, and the ratio of radiation to gas pressure remains constant (for each mass shell) throughout the period of adiabatic motion. The radiation diffuses sufficiently little during the period of acceleration that the flow can be modeled as adiabatic, although this approximation fails for the optically thin shell associated with the UV or X-ray flash (see, e.g., Ensman & Burrows 1992). The heat lost to radiation never exceeds a few percent of the total explosion energy, implying that radiative transfer can be neglected in general.

Under the approximation that the flow is adiabatic, radiation dominated, and nongravitating, its only dimensional scales are the explosion energy ($E_{\rm in}$), ejected mass ($M_{\rm ej}$), and initial stellar radius (R_*). Explosions with different values for these parameters, but the same initial density profile, are identical after rescaling the hydrodynamic variables by their characteristic values. Common stellar density profiles recur on a variety of scales, and the resulting (normalized) ejecta distributions are identical. We will make use of this principle in § 5.

We take a mass coordinate $m(r) \equiv M(r) - M_{\rm rem}$ (where $M_{\rm rem}$ is the mass of the material that will become the remnant) that is zero at the boundary between ejected and remnant material and increases to $M_{\rm ej}$ at the exterior. The configuration of the progenitor is specified by the initial

density $\rho_0(m)$ and the initial radius $r_0(m)$. If we normalize to the characteristic scales of mass, radius, velocity, time, density, pressure, and entropy, the flow expressed in normalized variables evolves independently of these scales. The basic characteristic scales are $M_{\rm ej}$, R_*, and $E_{\rm in}$, from which it is useful to derive the following characteristic quantities:

$$
\begin{aligned}
v_* &\equiv \sqrt{\frac{E_{\rm in}}{M_{\rm ej}}} = 2240\left(\frac{E_{\rm in}}{10^{51}\ {\rm ergs}}\right)^{1/2} \\
&\quad \times \left(\frac{M_{\rm ej}}{10\ M_\odot}\right)^{-1/2}\ {\rm km\ s^{-1}}\ , \\
t_* &\equiv R_*\sqrt{\frac{M_{\rm ej}}{E_{\rm in}}} = 1.552\times 10^4\left(\frac{R_*}{50\ R_\odot}\right) \\
&\quad \times \left(\frac{E_{\rm in}}{10^{51}\ {\rm ergs}}\right)^{-1/2}\left(\frac{M_{\rm ej}}{10\ M_\odot}\right)^{1/2}\ {\rm s}\ , \\
\rho_* &\equiv \frac{M_{\rm ej}}{R_*^3} = 4.720\times 10^{-4}\left(\frac{M_{\rm ej}}{10\ M_\odot}\right) \\
&\quad \times \left(\frac{R_*}{50\ R_\odot}\right)^{-3}\ {\rm g\ cm^{-3}}\ , \\
p_* &\equiv \frac{E_{\rm in}}{R_*^3} = 2.373\times 10^{13}\left(\frac{E_{\rm in}}{10^{51}\ {\rm ergs}}\right) \\
&\quad \times \left(\frac{R_*}{50\ R_\odot}\right)^{-3}\ {\rm ergs\ cm^{-3}}\ , \\
s_* &\equiv \frac{E_{\rm in}^{3/4}R_*^{3/4}}{M_{\rm ej}} = 2.278\times 10^{13}\left(\frac{E_{\rm in}}{10^{51}\ {\rm ergs}}\right)^{3/4} \\
&\quad \times \left(\frac{R_*}{50\ R_\odot}\right)^{3/4}\left(\frac{M_{\rm ej}}{10\ M_\odot}\right)^{-1}\ {\rm ergs^{3/4}\ cm^{3/4}\ g^{-1}}\ .
\end{aligned}
\tag{1}
$$

We will call the quantity $s \equiv p^{1/\gamma}/\rho$ the "entropy"; for $\gamma = 4/3$, it is proportional to the phase-space volume and the photon-to-baryon ratio.

The goal of this paper is to provide formulae for the end product of an adiabatic explosion. In the final state of adiabatic free expansion, the velocity of a given mass shell is fixed, while its density and pressure fall off as t^{-3} and $t^{-3\gamma} = t^{-4}$, respectively. The ejecta properties scale with the ejected mass, stellar radius, and blastwave energy: for a given feature in the ejecta (the half-mass shell, say),

$$
\begin{aligned}
v_f &\propto v_* = E_{\rm in}^{1/2}M_{\rm ej}^{-1/2}\ , \\
\rho_f &\propto \rho_*(t/t_*)^{-3} = E_{\rm in}^{-3/2}M_{\rm ej}^{5/2}t^{-3}\ , \\
p_f &\propto p_*(t/t_*)^{-4} = E_{\rm in}^{-1}M_{\rm ej}^2 R_*\, t^{-4}\ .
\end{aligned}
\tag{2}
$$

These overall scalings are very important for inferring gross quantities, but they say nothing about the relation between the progenitor's structure and the distribution of its ejecta.

So, we are interested here in the normalized ratios v_f/v_*, $\rho_f t^3/\rho_* t_*^3$, and $p_f t^4/p_* t_*^4$ as parameterized, for instance, by the normalized mass $m/M_{\rm ej}$. Note that these are "final" values only in the sense of an adiabatic explosion into vacuum: the radiation pressure will differ from $p_f t^4$ because of radiation diffusion and radioactive decay, and the distribution of matter in the ejecta [$v_f(m)$ and $\rho_f(m)t^3$] will ultimately be destroyed as interstellar material is swept up.

Throughout this paper, we use the normalized mass coordinate $\tilde{m} \equiv m/M_{\rm ej}$, which varies from 0 to 1 in the ejecta. Because all of the hydrodynamical variables approach power laws in the limit of high velocity, $\tilde{m} \to 1$, we introduce a notation that removes this dependence. In this limit, a variable x varies as $x \propto (1-\tilde{m})^{w_x}$ for some exponent w_x; so we define $f_x(\tilde{m})$ by

$$
x = x_*\, f_x(\tilde{m})(1-\tilde{m})^{w_x}\ , \tag{3}
$$

where x_* is a characteristic value for x (a combination of $E_{\rm in}$, $M_{\rm ej}$, and R_*). The exponents w_x and limiting coefficients $f_x(1)$ can be evaluated by combining the initial density and shock velocity in the subsurface layers with results from the planar, self-similar solution for the ejection of this material; this is done in § 5.1. Unless otherwise noted, f_x refers to the final value of x in free expansion. So, f_v refers to v_f, whereas f_{v_s} refers to v_s, the shock velocity.

3. STELLAR STRUCTURES OF THE PROGENITORS: STELLAR MODELS AND APPROXIMATIONS

The progenitors of core collapse supernovae are stars initially more massive than about 8 $M_\odot$ whose cores have advanced though carbon burning. The degenerate iron core approaches the Chandrasekhar mass in the subsequent burning stages, the process of "core convergence" (Arnett 1997). This core has the radius and density of an iron white dwarf. The circumnuclear shells decrease in density away from this core, characteristically as $\rho_0 \propto r_0^{-3}$. Outside the carbon shell, the helium envelope begins. There is typically a steep, shelflike decline in the density between the carbon and helium. The helium envelope is typically radiative prior to the explosion (Arnett 1997).

Above the helium envelope sits whatever hydrogen-rich envelope, which may be none at all, has survived the stellar mass loss. The structure of the star interior to the hydrogen is little altered by its presence or absence, because the hydrogen-burning shell has a pressure and a temperature that is negligible relative to those of the interior (Arnett 1997). In stars that have hydrogen, the boundary between hydrogen and helium is marked by a density drop even steeper and greater than at the base of the helium envelope. Presupernova stars with radiative hydrogen envelopes are blue supergiants (BSGs); those with convective hydrogen envelopes are red supergiants (RSGs); and those with no hydrogen at all are helium or carbon stars.

Core-collapse supernovae are classified observationally into Types II, Ib, and Ic. Type II supernovae show hydrogen lines, Type Ib show helium but no hydrogen, and Type Ic show neither. Because the spectrum may change with time, supernovae can shift in classification (Filippenko 1997): SN 1993J was one such example (see, e.g., Shigeyama et al. 1994). Thus red and blue supergiants have the capacity to produce Types II and Ib supernovae, helium stars can produce Types Ib and Ic, and carbon stars can produce only Type Ic.

We will concentrate on the topmost stellar envelope, which we will term the "outer envelope" and whose mass we designate $M_{\rm env}$. This layer is the hydrogen-rich envelope of those stars that have hydrogen. Those layers that lie interior to the outer envelope, but are also ejected in the explosion, we will refer to as the "mantle," with mass $M_{\rm man}$. The total ejecta mass $M_{\rm ej}$ is the sum of these, $M_{\rm ej} = M_{\rm man} + M_{\rm env}$. The "remnant," with mass $M_{\rm rem}$, is the stellar material that is not ejected; this is slightly greater than the

mass of the relict object because of rest energy radiated in the explosion. The total progenitor mass is $M_* = M_{\rm rem} + M_{\rm ej}$. Our focus on the outer envelope is motivated by the observation that it receives the lion's share of the explosion energy; moreover, our simulations indicate that the distribution of the outer envelope ejecta is determined primarily by its own structure and the mass $M_{\rm man}$ of the ejecta it overlies, but not appreciably by the structure of the underlying mantle material.

Convective envelopes, like those in RSGs, can be approximated as $n = 3/2$ polytropes in structure. This approximation would be exact if the convection were efficient, but the presence of a superadiabatic gradient breaks this idealization at large initial radii (Nomoto & Sugimoto 1972). Models of convection can prescribe a superadiabatic gradient, but the results depend on the model used (mixing length, for instance), as well as stellar parameters (such as $L_*/L_{\rm Edd}$). We will idealize convective outer envelopes as $n = 3/2$ polytropes, but the reader is advised to keep this caveat in mind.

Radiative envelopes of constant (Thomson-dominated) opacity, such as those in BSGs, limit to an effective polytropic index of $n = 3$ toward the outside of the star, because such envelopes behave like $n = 3$ polytropes when luminosity and mass are proportional. However, the interior of blue supergiants is better described by a lower effective polytropic index. In the BSG progenitor of Nomoto, we find that $2.1 < n_{\rm eff} < 2.4$ for the inner 75% of the ejected mass, with $n_{\rm eff}$ climbing to 3 in the exterior 25%. (A power law of index $17/7 = 2.43$ was adopted by Chevalier & Soker 1989.)

The structure of a polytropic envelope is determined, up to overall scaling factors, by a single parameter, corresponding to the fact that the Lane-Emden equation reduces to a first-order differential equation in terms of homology-independent variables (Chandrasekhar 1939). Which structure is appropriate is determined by the inner boundary condition, defined by the mantle's mass ratio $(M_{\rm man} + M_{\rm rem})/M_*$ and the radius ratio $R_{\rm man}/R_*$. In order to get a single parameter from these two, consider that the Lane-Emden equation describing the outer envelope can be integrated all the way to the center of the star. This hypothetical integration through the region actually occupied by the mantle will yield a polytrope that behaves as if it lay above a point mass at the origin. The value of the point mass compared to M_*, which we term q, provides a single parameter with which to distinguish outer envelope structures.

To understand the relation between q and the more familiar parameters $(M_{\rm man} + M_{\rm rem})/M_*$ and $R_{\rm man}/R_*$, we must examine the central behavior of polytropes. Polytropes with $n < 3$ limit as $r \to 0$ to the central distribution (Chandrasekhar 1939),

$$\rho_0 \propto (BR_*/r_0 - 1)^n , \tag{4}$$

for some constant $B \geq 1$ (equality when $q = 1$). In red supergiants ($n = 3/2$), one can typically ignore the envelope mass taken up by the volume of the mantle, both because the mantle radius is very small ($R_{\rm man} \simeq 1\% R_*$) and because the envelope mass is not highly concentrated toward the center ($\tilde{m} \propto r_0^{3/2}$). So, for RSGs, we can use the core-envelope mass ratio to parameterize the envelope structure:

$$q \simeq 1 - M_{\rm env}/M_* . \tag{5}$$

In BSGs, an effective value of q is less easily determined, because of the variation in the effective polytropic index $n_{\rm eff}$.

Polytropes with $q = 0$ extend continuously and smoothly to the origin, where $d\rho/dr = 0$ (because $dp/dr = 0$ at the center). For any value of q greater than zero, the central density profile is $\rho \propto r^{-n}$, as long as $n < 3$ (Chandrasekhar 1939). In polytropic envelopes that are much more massive than their cores, so that $q \ll 1$, this behavior is limited to a small region around the center (of similar mass), outside of which the structure returns to the flatter, $q = 0$ form. On the other hand, envelopes with $q \lesssim 1$ are dominated by the gravity of their cores: the density profile is everywhere at least as steep as the central behavior.

3.1. *Outer Density Distributions of Stars*

We will be especially interested in the region of a progenitor nearest the surface, because it is in this layer that the shock accelerates and casts away the highest velocity ejecta. Fortunately, the equations of polytropic stellar structure are simplified for this material. The hydrostatic equation for a polytropic envelope can be integrated to give

$$\rho_0^{1/n} = \rho_1^{1/n}\left(\frac{R_*}{r_0} - 1\right)\frac{\int_{r_*}^{1/r_0} [m(r) + M_{\rm rem}]dr^{-1}}{\int_{1/r_*}^{1/r_0} M_*\, dr^{-1}} , \tag{6}$$

where

$$\rho_1^{1/n} \equiv \frac{GM_*}{(n+1)KR_*} , \tag{7}$$

and $P_0 = K\rho_0^n$. In a shallow (outer) layer whose mass is negligible compared to M_*, the ratio of mass integrals is approximately unity. Therefore, this region has an analytical density structure:

$$\rho_0 = \rho_1\left(\frac{R_*}{r_0} - 1\right)^n . \tag{8}$$

This is valid only for masses such that the enclosed mass can be approximated by M_*; however, the region of validity may be relatively large in radius. For light envelopes whose entire mass is negligible ($q = 1$), this distribution holds for the entire envelope. Here, n is 3/2 for efficiently convective envelopes (although inefficient convection may invalidate this form) and exactly 3 for radiative envelopes of constant opacity (an analytical result in the outermost layers, where the ratio L/M is constant).

The stellar density coefficient ρ_1 is related to the mass coefficient $f_{\rho_0}(1)$, defined in equation (3), by the relation

$$f_{\rho_0}(1)^{n+1} = \frac{\rho_1}{\rho_*}\left(\frac{n+1}{4\pi}\right)^n ; \tag{9}$$

the corresponding exponent for ρ_0 as a power law in $(1 - \tilde{m})$ is

$$w_{\rho_0} = \frac{n}{n+1} . \tag{10}$$

For radiative envelopes of constant opacity,

$$\rho_1 = \frac{a(\mu m_{\rm H})^4}{192k_{\rm B}^4}\frac{G^3M_*^3}{R_*^3}\frac{\beta^4}{1-\beta} , \tag{11}$$

where $1 - \beta \equiv L_*/L_{\rm Edd}$ is the ratio of the stellar luminosity to the Eddington limit, or, equivalently, $1 - \beta$ is the ratio of

radiation pressure to total pressure in the outermost layers of the star. From equation (9), for radiative stars,

$$f_{\rho_0}(1) = 0.148\left(\frac{M_*}{M_{\rm ej}}\right)^{1/4}\frac{1-\beta}{\beta^{1/4}}\left(\frac{\mu}{0.62}\right)\left(\frac{M_*}{10\,M_\odot}\right)^{1/2}, \quad (12)$$

and for Thomson opacity,

$$1-\beta = \left(\frac{L_*}{3.86\times10^5\,L_\odot}\right)\left(\frac{M_*}{10\,M_\odot}\right)^{-1}\left(\frac{1+X_{\rm H}}{1.7}\right). \quad (13)$$

For convective envelopes with $0 < q < 0.9$, we find that,

$$f_{\rho_0}(1) \simeq \left(\frac{M_{\rm env}}{M_{\rm ej}}\right)^{2/5}(0.37 - 0.18q + 0.096q^2)\,. \quad (14)$$

This fit to the Lane-Emden solution is accurate to within 1% for the given range of q.

In summary, each layer of a star has a density distribution that is $\rho_0 \propto r_0^{-n}$ at its interior and that may flatten out toward constant density before dropping precipitously near the edge of the shell. The appropriate value of n is 3/2 for efficiently convective envelopes and 2.1–3 for radiative envelopes. Besides n, the structure of a polytropic envelope depends on a central concentration parameter q; for the outer envelopes of RSGs, q is essentially the mass interior to the envelope divided by the progenitor mass. There are sharp drops in density between the carbon and helium and between the helium and hydrogen shells; the latter is most drastic in the case of red supergiants.

4. MODEL FOR SHOCK PROPAGATION

It is through this layered sequence of envelopes that the supernova shock propagates. A model for the shock velocity must account for the general deceleration as mass is swept up, punctuated by accelerations as the shock encounters steep density gradients. The velocity of the blastwave shock is clearly affected by all of the material it has encountered, as well as the conditions at the shock front. However, the history of analytical shock-velocity approximations has primarily been the search for a combination of local variables that controls (or at least mimics) the motion of the front. Formulae in the literature have typically given v_s in terms of the local initial density ρ_0 and radius r_0, as well as the blastwave energy, $E_{\rm in}$ (an integral quantity).

4.1. *Previous Models*

Kompaneets (1960) considered shock acceleration in the case of an initially exponential density distribution. He approximated the postshock pressure as a constant fraction of the mean energy density, leading in the case of spherical symmetry and in our notation to the expression

$$\frac{v_s}{v_*} = \Gamma_{\rm K60}\left(\frac{\rho_0}{\rho_*}\right)^{-1/2}\left(\frac{r_0}{R_*}\right)^{-3/2}, \quad (15)$$

where $\Gamma_{\rm K60}$ is a constant that can be evaluated in specific cases. As discussed by Koo & McKee (1990), this approximation overestimates the shock velocity as the shock accelerates, both because the mean pressure drops in relation to the mean energy density, and because the postshock pressure drops in relation to the mean pressure. Laumbach & Probstein (1969) developed an approximation for the motion of the shock wave in which the shocked material is assumed to be concentrated in a thin shell behind the shock, moving at the postshock velocity. The approximation involved Taylor expansions for the form of this shell, and related these to the motion of the shock. As Koo & McKee (1990) discuss, this approximation tends to underestimate the shock velocity and fails for strongly accelerating shocks.

Klimishin & Gnatyk (1982) considered shocks that alternate between periods of deceleration and acceleration, as shocks in supernovae do. They proposed that the shock velocity should obey $v_s \propto E_{\rm in}^{1/2}(\rho_0 r_0^3)^{-1/2}$ during periods of deceleration and $v_s \propto E_{\rm in}^{1/2}(\rho_0 r_0^3)^{-\beta_1}$ (with $\beta_1 = 0.2$) during periods of acceleration.

Koo & McKee (1990), considering density distributions that steepen monotonically, proposed a shock velocity that accelerates beyond a characteristic radius. Specifically, they chose a postshock pressure that changes from the form appropriate to spherical, decelerating blastwaves (as in Sedov 1959) to that appropriate to strongly accelerating blastwaves (as in Whitham 1974) at a transition radius $R_{s,t}$. This leads to the shock velocity formula,

$$\frac{v_s}{v_*} = \Gamma_{\rm KM90}\left(\frac{\rho_0}{\rho_*}\right)^{-\beta_1}\left(\frac{r_0}{r_0+R_{s,t}}\right)^{-3/2}\left(\frac{r_0+R_{s,t}}{R_{s,t}}\right)^{-\beta_2}, \quad (16)$$

where $\Gamma_{\rm KM90}$ is a coefficient chosen to match Sedov-Taylor blastwave if the central density distribution is flat. This prescription worked well for the relatively smooth distributions considered, which were flat at the origin and fell to zero density asymptotically at large radii with a well-defined scale length.

However, supernova progenitors have layers of different compositions, separated by shelflike drops in density at the burning shells (§ 3). Therefore one must employ a model for shock acceleration that does not rely on the choice of a single radial scale. The ability to match the acceleration of the shock in the interior shell boundaries and at the outer edge of the star is particularly essential.

4.2. *Improved Model for Shock Velocity*

During a period of self-similar shock propagation (see, e.g., Sedov 1959), the shock velocity obeys $v_s \propto [E_{\rm in}/m(r_0)]^{1/2}$. During this period, as well, the ratio $\rho(r_0)/\overline{\rho}(r_0)$ is a constant, where $\overline{\rho}(r_0)$ is the average density of the material to be ejected within r_0 (note that $\overline{\rho}$ and $\tilde{m}$ do not include the stellar core mass that will become the remnant object). During a period of strong planar acceleration, when r_0 and $m(r_0)$ are essentially constant [and so $\overline{\rho}(r_0)$ is, too], the shock velocity takes the form $v_s \propto [\rho(r_0)/\overline{\rho}(r_0)]^{-\beta_1}$. We propose a continuous and simple form. To accommodate both spherical deceleration and planar acceleration, we take the product form $v_s \propto [E_{\rm in}/m(r_0)]^{1/2}[\rho_0(r_0)/\overline{\rho}_0(r_0)]^{-\beta_1}$:

$$\frac{v_s}{v_*} = \Gamma\tilde{m}^{\beta_1-1/2}\left(\frac{\rho_0}{\rho_*}\right)^{-\beta_1}\left(\frac{r_0}{R_*}\right)^{-3\beta_1}. \quad (17)$$

Using the approximation that a strongly accelerating shock runs along a forward characteristic of the postshock flow, Whitham obtained $\beta_1 \simeq 1/\{2+[2\gamma/(\gamma-1)]^{1/2}\}$, or 0.2071 for $\gamma = 4/3$. The self-similar, planar solution of Gandel'man & Frank-Kamenetsky (1956) and Sakurai (1960) gives $\beta_1 = 0.1909$ and $\beta_1 = 0.1858$ for $n = 3/2$ and $n = 3$, respectively, so $\beta_1 \simeq 0.19$ is a reasonable approximation. (Note that in writing eqs. [15], [16], and [17] for v_s/v_*, we have sup-

pressed the explicit dependence $v_s \propto E_{\rm in}^{1/2}$ that is important for blastwaves whose energy is not conserved.)

It is possible to define $\Gamma(r_0)$ in terms of moments of the distribution $\rho_0(r < r_0)$ in such a way as to make equation (17) strictly correct for self-similar blastwaves. For a self-similar blastwave in the distribution $\rho_0 \propto r_0^{-k_\rho}$, equation (17) is correct if $\Gamma = \sigma^{-1/2}[4\pi/(3 - k_\rho)]^{-\beta_1}$, where $\sigma = E_{\rm in}/(mv_s^2)$. For the Primakoff blastwave, $\sigma = 8/[3(\gamma + 1)^2]$, so that

$$\Gamma = \frac{7}{\sqrt{24}}(7\pi)^{-\beta_1} \tag{18}$$

for $\gamma = 4/3$. Radiative stars roughly resemble the Primakoff power law $\rho_0 \propto r_0^{-17/7}$ (Chevalier & Soker 1989), as do the mantles of RSGs. Despite the actual differences between stellar distributions and this power-law form, we find that, together, equations (17) and (18) are remarkably accurate (Fig. 2).

Throughout the bulk of the stellar mantle and envelope in our simulations, the exact choice of β_1 between the self-similar or approximate values makes very little difference. However, the exact values are important for determining the power laws of high-velocity ejecta (§ 5.1). We find typical errors of v_s in the stellar envelope to be $\sim 2\%$, although they are higher ($\sim 10\%$) in the mantle and in regions of strong acceleration. However, these errors are in comparison to simulations of adiabatic, nongravitating point explosions in a gas sphere of mass $m(R_*) = M_* - M_{\rm rem}$. In real supernovae, the shock velocity will differ significantly from this formula at the base of the ejecta, because, in part, of the mass that ultimately enters the remnant; in particular, the shock velocity does not approach infinity as $m \to 0$, contrary to equation (17). Our focus is on the envelope and outer mantle, however, and for these equation (17) should remain accurate.

Taking the value $\beta_1 \simeq 0.19$ to represent both radiative and convective envelopes, we can write equation (17) as

$$v_s \simeq 0.794 v_* \tilde{m}^{-0.31}\left(\frac{\rho_0}{\rho_*}\right)^{-0.19}\left(\frac{r_0}{R_*}\right)^{-0.57}$$
$$= 0.794\left(\frac{E_{\rm in}}{m}\right)^{1/2}\left(\frac{m}{\rho_0 r_0^3}\right)^{0.19}, \tag{19}$$

where m is the enclosed ejecta mass.

To summarize the shock velocity approximations: the Kompaneets approximation has $v_s \propto E^{1/2}\rho_0^{-1/2}r_0^{-3/2}$, corresponding to a constant ratio of postshock to mean pressure. The Koo & McKee (1990) approximation goes from $v_s \propto E_{\rm in}^{1/2}\rho_0^{-\beta_1}r_0^{-3/2}$ to $v_s \propto E_{\rm in}^{1/2}\rho_0^{-\beta_1}r_0^{-\beta_2}$ at a transition radius $R_{s,t}$. Klimishin & Gnatyk took $v_s \propto E_{\rm in}^{1/2}(\rho_0 r_0^3)^{-1/2}$ and $v_s \propto E_{\rm in}^{1/2}(\rho_0 r_0^3)^{-\beta_1}$ in periods of deceleration and acceleration, respectively. Our approximation has $v_s \propto E^{1/2}m^{\beta_1 - 1/2}\rho_0^{-\beta_1}r_0^{-3\beta_1}$. By introducing m and using ρ_0 and r_0 only in the combination $\rho_0 r_0^3$, we avoid having to choose dimensional scales. We compare the Kompaneets, Klimishin, & Gnatyk and Koo & McKee approximations to our equation (17) in Figure 2.

Equation (17) represents an improved approximation for v_s in terms of the initial quantities m, r_0 and ρ_0, and $E_{\rm in}$. These Lagrangian variables are especially convenient because they are readily available in the initial state. Including m allows the dimensionless ratio $\rho_0(r_0)/\overline{\rho}_0(r_0)$ to enter

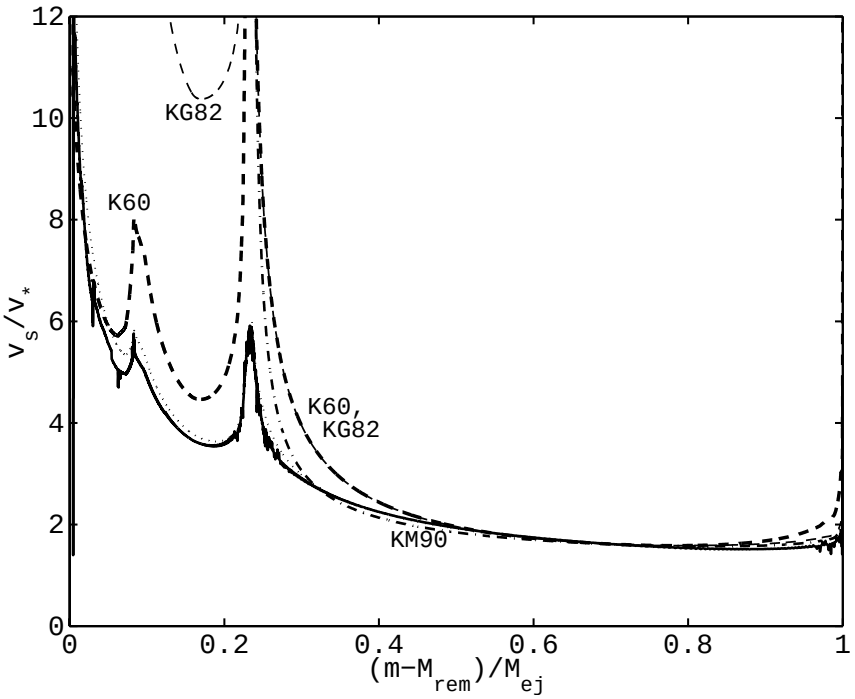

FIG. 2.—Forward shock velocity in a numerical simulation of the 15 $M_\odot$ RSG progenitor S15A of Woosley & Weaver (1995; *solid line*), and a comparison between our shock velocity formula (eq. [17]; *dotted line*) and the formulae of Kompaneets (1960; *thick dashed line*), Klimishin & Gnatyk (1982; *thin dashed line*), and Koo & McKee (1990; *dot-dashed line*). Except for our formula, shock velocities have been normalized to match the numerical value at $\tilde{m} = 0.7$. The constant $R_{s,t}$ in the model of Koo & McKee has been chosen to optimize the shock velocity in the outer envelope. To be fair, ours is the only formula designed specifically for the context of supernovae.

into the shock-velocity approximation. Whereas the shock velocity must in reality depend on the detailed structure of the material encountered so far, it appears as if this single moment of the initial density distribution is sufficient to specify the shock velocity quite accurately.

It is important to note that equation (17) is a purely local theory for the shock velocity, in the sense that it makes reference only to the variables (m, r_0, ρ_0) at the same mass shell in the progenitor.

In the upcoming sections, we will be interested in relating the ejecta pressure to its density by means of the "entropy," $s(\tilde{m}) = p^{1/\gamma}/\rho$. Using equation (17) with $\gamma = 4/3$, we can specify the entropy of material that experiences no reverse shock:

$$\frac{s(\tilde{m})}{s_*} = \frac{6^{3/4}}{7^{7/4}}\,\Gamma^{3/2}\left[\frac{\rho_0(\tilde{m})}{\rho_*}\right]^{-(1+6\beta_1)/4}\left[\frac{r_0(\tilde{m})}{R_*}\right]^{-9\beta_1/2}\tilde{m}^{(6\beta_1-3)/4}. \tag{20}$$

This entropy formula, like the shock-velocity formula from which it is derived, is a local theory, invoking only (m, r_0, ρ_0) for the same mass shell of the progenitor. It falls short for shells that will encounter a strong reverse shock, a weakness that will prevent our models from describing the mantle ejecta accurately. Including reverse shocks would require more information than the local variables (m, r_0, ρ_0) provide.

5. HIGH-VELOCITY EJECTA

The analytical outer-density distribution described in § 3.1 provides a stable platform from which to launch a study of envelope expulsion in supernovae. The fact that polytropic envelopes of the same index share this common form is useful for understanding how a planar, self-similar analog is applicable to the shock and rarefaction flow in this region. Moreover, this distribution allows a characterization of the way in which the real, spherical flow differs from the planar analog.

For material that is close enough to the stellar surface, ($R_* - r_0 \ll R_*$), the density distribution of equation (8) takes the limit $\rho_0 \to \rho_1(1 - r_0/R_*)^n$. If a mass shell stays in this small range of radii throughout its period of acceleration, spherical curvature will not affect its dynamics. Then, its velocity will be set by the planar, self-similar problem first posed by Gandel'man & Frank-Kamenetsky (1956) and solved by Sakurai (1960), which we reconsider in the Appendix. The material covered by this solution settles into power-law distributions whose indices are easily derived once the shock velocity index β_1 is known (cf. Chevalier & Soker 1989). If the coefficients of density [ρ_1 or $f_{\rho 0}(1)$] and shock velocity are known, the coefficients of the final density distributions can also be derived (cf. Imshennik & Nadëzhin 1989). In § 5.1 the indices and coefficients of this high-velocity material are calculated, using the results of § 4 to set the shock-velocity coefficient.

This planar, self-similar analog is limited in its applicability to real supernovae by several effects. For mass shells that differ appreciably in radius from R_*, ρ_0 is no longer a simple power law in depth. For such shells, changes in radius are also sure to make a planar approximation poor. In fact, as first mentioned by Litvinova & Nadëzhin (1990), curvature is actually negligible only when $(1 - r_0/R_*)^{1/3} \ll 1$, not just when $(1 - r_0/R_*) \ll 1$, because acceleration is very slow in the planar solution.

The postshock and rarefaction flow are profoundly affected by sphericity, but in a way that is consistent among different progenitors. The effects that corrupt the planar solution are primarily geometrical in nature—that is, they occur because of differences in the initial distribution (with scale length R_*) or differences in the hydrodynamics (also with scale length R_*). Insofar as the initial distributions of material are identical after rescaling (i.e., so long as eq. [8] is correct), the fully spherical processes of shock propagation and expansion in different progenitors are identical. This implies that the outer ejecta distributions of polytropes share common forms, which limit to the self-similar power-law solutions at the highest velocities. Specifically, one can multiply these power laws by a function that depends on the initial depth, in order to account for the effects of progenitor structure and spherical expansion. The validity of this approach is demonstrated in § 5.2, where such correction factors are also presented. This approach is similar to the analytical solution of Kazhdan & Murzina (1992), who present a correction factor (parameterized by γ and n) that accounts for the first-order effect of sphericity at all times in the flow. As shown in the Appendix, the correction factors we derive resemble the outcome of the suggestion by Litvinova & Nadëzhin (1990) that spherical effects truncate planar expansion once the radius has expanded by a certain amount (of order R_*).

To put it another way, it is possible to define a set of variables that remove the scalings of physical quantities in the outer edge of a star. In terms of these variables, polytropes of the same index assume the same structure (no longer up to a multiplicative constant) at large initial radii, and, since the new time and velocity variables have taken out variations in the strength of the shock as it enters the outermost regions, different polytropic progenitors play out the same behavior of shock acceleration and outer envelope ejection—a behavior that includes the effects of the finite radius on the initial conditions and on the hydrodynamics of spherical expansion. Equation (8) demonstrates that the normalized initial radius r_0/R_* [or the normalized initial depth, $x_0 \equiv (R_* - r_0)/R_*$] and the rescaled mass coordinate $(1 - \tilde{m})/(\rho_1/\rho_*)$ are variables of the required type, as is the density variable ρ/ρ_1. (The results in the Appendix, as well as the analytical development of Kazhdan & Murzina 1992, show that the variable $x_0^{1/3}$ is more relevant than x_0, and so we define the corresponding mass variable $\delta\hat{m} \equiv [(1 - \tilde{m})/(\rho_1/\rho_*)]^{1/3(n+1)}$.) For the shock strength, we must rely on the results of § 4 to generate a new velocity variable $(v/v_*)(\rho_1/\rho_*)^{\beta_1}$ that removes the scaling of shock velocity with the structure of the star. In terms of these variables, the final distribution of high-velocity ejecta from polytropes of the same index n share a single distribution, which need be determined only once. Since it is convenient to write this distribution as a power law (the self-similar result) times a correction factor, it is natural to express the correction factor in terms of $x_0^{1/3}$, $\delta\hat{m}$, or $(v_f/v_*)(\rho_1/\rho_*)^{\beta_1}$, as is done in § 5.2.

However, such correction factors must themselves fail to describe the ejecta at some depth, or for velocities that are too low. This follows from the fact that equation (8) is valid only in the region for which the enclosed mass is essentially M_*. For radiative envelopes of constant opacity, the effective polytropic index deviates from 3 for the interior mass shells. For polytropes as well, the initial density distribution is affected: the actual density distribution (eq. [6]) differs

from the common distribution (eq. [8]) when $m(r) + M_{\rm rem} < M_*$. Even when the shock wave is in the outermost mass zones, its velocity is still being affected by the forward characteristics of the earlier blastwave flow. At what point does the flow forget its history and limit to a common distribution in these outer regions? Theory (Whitham 1974) suggests that a shock's velocity behavior is determined by local conditions once it begins to accelerate strongly. The approach adopted in § 5.2 is to determine numerically what region of the ejecta is reproduced by a variety of progenitors and to present fits for correction factors only in this region.

There is an upper velocity limit on the validity of our solutions as well, because the finite width of the radiative shock becomes comparable to the depth at some point. Our assumption of adiabatic flow must break down by this point. We estimate the maximum velocity in § 5.3.

5.1. *Limiting Power Laws for the Highest Velocity Ejecta*

From our shock-velocity approximation and the resulting entropy distribution, equations (17) and (20), the outer coefficients of shock velocity and entropy are, for $\gamma = 4/3$,

$$f_{v_s}(1) = \Gamma f_{\rho_0}(1)^{-\beta_1}\,,$$
$$f_s(1) = 0.1273\Gamma^{3/2} f_{\rho_0}(1)^{-(3\beta_1/2+1/4)}\,. \tag{21}$$

In the planar, self-similar solution, $v_f(\tilde{m})/v_s(\tilde{m})$ is a constant, $(v_f/v_s)_{\rm p}$, whose value we derive in the Appendix and present in Table 2. This ratio gives $f_v(1)$ from $f_{v_s}(1)$; then, mass continuity and entropy conservation give $f_\rho(1)$ and $f_p(1)$:

$$f_v(1) = f_{v_s}(1)\left(\frac{v_f}{v_s}\right)_{\rm p}\,,$$
$$f_\rho(1) = \frac{1}{4\pi}\left(\frac{n+1}{\beta_1 n}\right) f_{\rho_0}(1)^{3\beta_1}\left(\frac{v_f}{v_s}\right)_{\rm p}^{-3}\,,$$
$$f_p(1) = 0.002191\left(\frac{n+1}{\beta_1 n}\right)^{4/3}\Gamma^{-2} f_{\rho_0}(1)^{2\beta_1-1/3}\left(\frac{v_f}{v_s}\right)_{\rm p}^{-4}\,. \tag{22}$$

The exponents of these variables in $(1-\tilde{m})$ are easily derived, but we state them here for convenience (the values are given in Table 2):

$$w_v = w_{v_s} = -\beta_1 w_{\rho_0} = -\beta_1\left(\frac{n}{n+1}\right),$$
$$w_s = \left(\frac{1}{\gamma}-1\right)w_{\rho_0} + \frac{2}{\gamma}\,w_v = \frac{n}{\gamma(n+1)}\,(1-2\beta_1-\gamma)\,,$$
$$w_\rho = 1 - 3w_v = 1 + 3\beta_1\left(\frac{n}{n+1}\right),$$
$$w_p = \gamma(w_s + w_\rho) = \frac{\gamma + n - 2\beta_1 n + 3\beta_1\gamma n}{n+1}\,. \tag{23}$$

As an example, the asymptotic velocity distribution is

$$v_f(\tilde{m}\to 1) = f_v(1)(1-\tilde{m})^{w_v} v_* = \Gamma\left(\frac{v_f}{v_s}\right)_{\rm p} f_{\rho_0}(1)^{-\beta_1}(1-\tilde{m})^{-\beta_1 n/(n+1)} v_*\,. \tag{24}$$

The asymptotic final density and pressure distributions are given in terms of velocity by $\rho_f \propto v_f^{l_{\rho 2}} t^{-3}$ and $p_f \propto v_f^{l_{p2}} t^{-4}$, where

$$l_{\rho 2} = \frac{w_\rho}{w_v} = -\frac{n+1+3\beta_1 n}{\beta_1 n}\,,$$
$$l_{p2} = \frac{w_p}{w_v} = -\frac{\gamma + n + \beta_1 n(3\gamma-2)}{\beta_1 n}\,. \tag{25}$$

(The subscript 2 denotes power laws for the outer ejecta—see § 7.) The values for $n = 3/2$ and $n = 3$ are given in Tables 4 and 5, respectively. Based on comparison with actual stellar models (§ 9), there is some indication that even when the local value of $n_{\rm eff} \equiv d\log\rho_0/d\log x_0$ varies, equation (25) still roughly approximates $d\log\rho_f/d\log v_f$ and $d\log p_f/d\log v_f$ for the high-velocity ejecta of peripheral material. Note that a shallower initial density produces a steeper final density and pressure in the outermost ejecta.

5.2. *Common Spherical Dynamics of High-Velocity Ejection*

In Figures 3 and 4 we demonstrate that convective and radiative stellar envelopes indeed each assume a common exterior distribution, as discussed above; that the shock velocity approaches a common form for each (up to a constant); and that the ratio $v_f(r_0)/v_s(r_0)$ does as well. In the Appendix we investigate the implications of the suggestion of Litvinova & Nadëzhin (1990) that the final velocity is set by the truncation of planar, self-similar acceleration once a shell's radius has expanded to a radius somewhat larger than R_*. This, along with the form of the self-similar dynamics (eq. [A5]) gives a form for v_f/v_s, equation (A7), that is a polynomial in $x_0^{1/3}$, where $x_0 \equiv 1 - r_0/R_*$ is the normalized depth. It is no surprise, then, that the numerically determined distribution of $v_f(r_0)/v_s(r_0)$ is best fit and expressed as a function of $x_0^{1/3}$ (as shown analytically by Kazhdan & Murzina 1992):

$$\frac{v_f(x_0)}{v_s(x_0)} \simeq \left(\frac{v_f}{v_s}\right)_{\rm p}(1 - 0.51x_0^{1/3} + 0.76x_0^{2/3} - 1.19x_0) \qquad (n = 3/2)\,,$$
$$\frac{v_f(x_0)}{v_s(x_0)} \simeq \left(\frac{v_f}{v_s}\right)_{\rm p}(1 - 0.34x_0^{1/3} + 0.24x_0^{2/3} - 0.37x_0) \qquad (n = 3)\,, \tag{26}$$

TABLE 2

QUANTITIES ASSOCIATED WITH SELF-SIMILAR, PLANAR EXPANSION

Quantity	$n = 3/2$	$n = 3$	Comments
λ	0.2863	0.5573	Method of Sakurai 1960
β_1	0.1909	0.1858	Method of Sakurai 1960
	0.2071	0.2071	Approximation of Whitham 1974
$\left(\frac{v_f}{v_s}\right)_{\rm p}$	2.1649	2.0351	Derived in Appendix
w_{ρ_0}	3/5	3/4	Initial density distribution
w_{v_s}	−0.1145	−0.1394	Eq. (23)
w_s	−0.3218	−0.3965	Eq. (23)
w_ρ	1.3436	1.4181	Eq. (23)
w_p	1.3624	1.3624	Eq. (23)

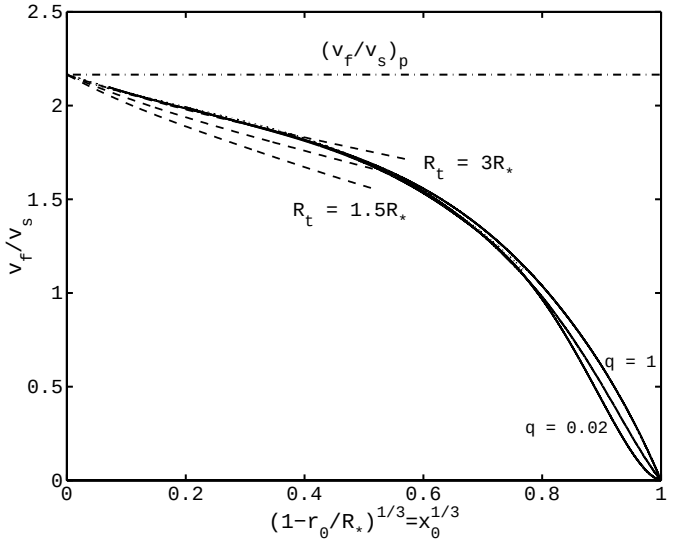

FIG. 3.—Ratio of shock velocity to final velocity for a sequence of simulated explosions in polytropes without mantles (index $n = 3/2$; $q = 0.02$, 0.3 and 1), parameterized by the radial variable $x_0^{1/3}$. If the progenitors were homologous copies of one another, dimensionless quantities such as this would not vary. The progenitors are most similar at the outermost radii, a feature that holds for this ratio as well. The ratio in each simulation approaches the planar, self-similar value (*dot-dashed line*). The suggestion of Litvinova & Nadëzhin (1990) that spherical expansion may truncate self-similar expansion at a radius R_t gives a definite prediction of the variation of this ratio with depth (*dashed lines*, for $R_t = 1.5$, 2 and $3R_*$). Our fit to the dependence of v_f/v_s with x_0 is also plotted (eq. [26]; *dotted line*).

where $(v_f/v_s)_p$ is given in Table 2. These fits were made to the outer one-half of the radius of the $q = 0.3$ polytrope in each case. The fit for $n = 3/2$ is good to within 1% for $r_0 > 0.55$ for both $q = 0$ and $q = 0.3$ and to within 3% for $r_0 > 0.2$ for $q = 1$ polytropic envelopes. The fit for $n = 3$ is good to within 1% for $r_0 > 0.5$, 0.6, and 0.65 for $q = 0.3$, $q = 0$, and $q = 1$, respectively. As shown in Figure 3, the full spherical result, equation (26), resembles the outcome of Litvinova & Nadëzhin's suggestion, equation (A7), if acceleration halts at about $3R_*$.

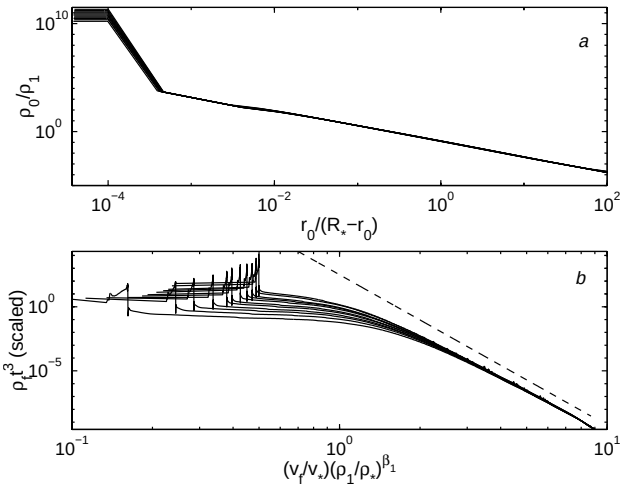

FIG. 4.—Similarity of the outer regions of polytropic envelopes is reproduced as similarity of the high-velocity ejecta. (*a*) The sequence of polytropic progenitors used to simulate red supergiants (§ 8), plotted as normalized initial density ρ_0/ρ_1 against the variable $r_0/(R_* - r_0)$, in which ρ_0/ρ_1 is a power law for the region in which polytropic envelopes share a common form (§ 3.1). (*b*) The ejecta distribution produced in these models: normalized final density against normalized final velocity. For comparison, the self-similar planar power law (*dashed line*) is also shown.

We note that the first-order correction terms in equation (26) are predicted by the analytical perturbation theory of Kazhdan & Murzina (1992). From their theory, the first-order coefficient should be -0.3253 for $n = 3$ above, where we find -0.34 in our fit. The two coefficients are somewhat different in meaning, in that the Kazhdan & Murzina coefficient represents a term in the expansion of v_f/v_s around $x_0^{1/3} = 0$, whereas ours is part of a cubic polynomial fit to a range of the variable $x_0^{1/3}$. The value -0.3252 for the first term in this expansion implies that planar acceleration of the outermost material is effectively truncated at $2.94R_*$ in Litvinova & Nadëzhin's scenario, very close to our estimate of $3R_*$ (see the Appendix).

In the region for which envelopes of the same value of n scale to a common solution, we can give the Lagrangian form of the ejecta distributions, i.e., $v_f(\tilde{m})$, $\rho_f(\tilde{m})t^3$, and $p_f(\tilde{m})t^4$. We present these high-velocity formulae in Table 3. These formulae consist of the power laws derived in § 5.1, multiplied by a function of mass that accounts for the deviations from self-similar flow. Since the mass external to a depth x_0 is $1 - \tilde{m}(x_0) = 4\pi x_0^{n+1}(\rho_1/\rho_*)/(n + 1)$, the mass variable corresponding to $x_0^{1/3}$ can be defined as

$$\delta\hat{m} \equiv [(1 - \tilde{m})(\rho_1/\rho_*)^{-1}]^{1/3(n+1)} . \quad (27)$$

This variable is convenient for giving the correction factors to power laws in $(1 - \tilde{m})$, as in Table 3, because the effects of spherical expansion are linear in $\delta\hat{m}$ just as they are in $x_0^{1/3}$.

5.3. *Shock Breakout and the Maximum Ejecta Velocity*

When a supernova shock approaches the surface of the star, there comes a point at which the postshock radiation can leak out in a burst of ionizing radiation (see, e.g., Klein & Chevalier 1978; Chevalier & Klein 1979). This event marks the end of shock acceleration and limits the velocity at which ejecta can be cast away. The shock velocity at breakout is well-determined from simple considerations. This sets both the upper velocity limit for the assumption of adiabatic flow and the gross properties of the radiation outburst (Imshennik & Nadëzhin 1989).

Shock propagation is unaffected by the leakage of radiation until the optical depth of the shock exceeds the optical depth of the available material. Since the shock wave is a region in which light diffuses upstream and gets amplified by compression, the time for light to diffuse across the shock front must be comparable to the time for material to flow through it. This equality sets the physical size of the shock transition: a simple estimate shows that the shock's optical depth is

$$\tau_s \simeq \frac{c}{v_s} . \quad (28)$$

This is only an approximate equality, because the shock structure set by radiation diffusion is not sharp. In fact, the structure of a strong, radiation-dominated shock front propagating into a uniform medium can be calculated analytically using the diffusion approximation (Weaver 1976).

TABLE 3

FORMULAE FOR HIGH-VELOCITY DISTRIBUTIONS OF EJECTA QUANTITIES

Quantity	High-Velocity Formula	Validity
Convective Outer Envelopes ($n = 3/2$)		
v_f/v_*	$2.06(\rho_1/\rho_*)^{-0.08}(1-\tilde{m})^{-0.1145}(1+0.30\ \delta\hat{m})$	$\delta\hat{m} \lesssim 0.8$
$\rho_f t^3/\rho_* t_*^3$	$0.079(\rho_1/\rho_*)^{-0.23}(1-\tilde{m})^{1.344}(1+0.67\ \delta\hat{m})$	$\delta\hat{m} \lesssim 0.8$
$p_f t^4/p_* t_*^4$	$0.0027(\rho_1/\rho_*)^{0.02}(1-\tilde{m})^{1.362}(1+0.96\ \delta\hat{m})$	$\delta\hat{m} \lesssim 0.7$
Radiative Outer Envelopes ($n = 3$)		
v_f/v_*	$1.92(\rho_1/\rho_*)^{-0.05}(1-\tilde{m})^{-0.1394}(1-0.23\ \delta\hat{m}-0.095\ \delta\hat{m}^2)$	$\delta\hat{m} \lesssim 0.9$
$\rho_f t^3/\rho_* t_*^3$	$0.081(\rho_1/\rho_*)^{0.14}(1-\tilde{m})^{1.418}(1+0.49\ \delta\hat{m}+0.61\ \delta\hat{m}^2)$	$\delta\hat{m} \lesssim 0.9$
$p_f t^4/p_* t_*^4$	$0.0026(\rho_1/\rho_*)^{0.01}(1-\tilde{m})^{1.362}(1+1.03\ \delta\hat{m}+0.37\ \delta\hat{m}^2)$	$\delta\hat{m} \lesssim 0.75$

NOTE.—Final distributions depend on the parameter ρ_1/ρ_* defined by eq. (8), describing the subsurface layers of the progenitor (§ 3.1). Characteristic values such as v_* are combinations of the ejecta mass, energy, and radius (§ 2). For each quantity, the distribution limits to a power law at the highest velocities. The factor that depends on $\delta\hat{m}$ describes the deviation from this power law toward lower velocities, primarily because of the onset of spherical expansion. Here, $\delta\hat{m} \equiv [(1-\tilde{m})(\rho_1/\rho_*)^{-1}]^{1/3(n+1)}$. These formulae are valid in the region for which envelopes of the same value of n, but different internal structures, share a common form in numerical simulations. Significant digits are apportioned according to accuracy: most accurately determined are the power-law exponents, i.e., the exponents on $(1-\tilde{m})$.

In this solution, the radiation pressure varies with optical depth as

$$\frac{p}{\rho_0 v_s^2} = \frac{6\ \exp\left[-3(\tau-\tau_0)v_s/c\right]}{1+7\ \exp\left[-3(\tau-\tau_0)v_s/c\right]}, \tag{29}$$

where τ is the optical depth (increasing inward) and τ_0 is a constant that defines the position of the shock front. Here, the radiation pressure approaches its upstream and downstream asymptotes exponentially. However, the smoothness of the shock front introduces little uncertainty into the velocities ($\sim 20\%$) and temperatures ($\sim 10\%$) derived below (Imshennik & Nadëzhin 1989).

Shock breakout occurs when τ_s is equal to the stellar optical depth $\tau(x_0)$ at some depth x_0:

$$\tau(x_0) = \frac{\kappa\rho_1 R_* x_0^{n+1}}{n+1}, \tag{30}$$

or, equivalently, when the radiation diffusion time across the shock front equals the time for the shock to get to the stellar surface (the local dynamical time). The terminal shock velocity v_s(breakout) at this point, where $\tau_s = \tau(x_0)$, is, from equations (17), (28), and (30),

$$v_s(\text{breakout}) \simeq \Gamma v_* \left[\left(\frac{\rho_1}{\rho_*}\right)^{-1/n}\left(\frac{\Gamma}{1+n}\right)\left(\frac{v_*}{c}\right) \times \left(\frac{\kappa M_{\rm ej}}{R_*^2}\right)\right]^{\beta_1 n/(1+n-\beta_1 n)}. \tag{31}$$

The breakout shock velocity scales most significantly with v_*, because β_1 is a small number.

It is interesting to note that the width of the shock at the time of breakout is about $0.014R_*$ and $0.019R_*$ for RSGs and BSGs, respectively. So, the parameter $x_0^{1/3}$ is at least 0.24 and 0.27, respectively, for the adiabatic ejecta. Therefore the planar, self-similar limit is never strictly achieved.

5.3.1. *The Speed Limit for Supernova Ejecta*

One might expect that, after breakout, the diffusion of radiation would interfere with adiabatic expansion at lower and lower velocities. If this were true, even those mass shells not involved in the shock at the time of breakout would be affected, and our adiabatic results would not be applicable to these shells.

However, a straightforward comparison of the diffusion time ($\sqrt{3}\tau^2/c\kappa\rho$) and the dynamical time [$t - t$(breakout)] for a particular mass shell shows that this does not actually happen. Instead, the adiabatic approximation holds for mass shells deeper than a few shock widths from the surface at the time of breakout.

To see this, consider the phase of planar free expansion, when a mass shell has traveled far compared to its initial depth but only a small distance relative to R_*. Then, because the surface area of a shell is effectively constant, the density scales as $\rho(m) \propto 1/[t - t(\text{breakout})]$. Since the optical depth τ of a mass shell does not vary in planar flow, the diffusion time is proportional to the dynamical time during this planar free expansion phase. Examining the planar, self-similar solution presented in the Appendix, we find that the ratio of the local diffusion time to dynamical time is never less than its value in free expansion. Similarly, the shock front itself has a width that is set by the equality of the diffusion time across the front to the time for material to cross the shock front. As a result, the criterion for a mass shell to experience significant radiation diffusion during planar expansion is simply that it be entrained in the shock at the time of breakout.

Even so, one might still worry that the onset of spherical expansion will permit a diffusion wave to propagate inward. Then, the geometric reduction of a mass shell's velocity would be enhanced (and the formulae of § 5.2 invalidated) by the loss of photons. Fortunately, this does not happen either. The results of § 5.2 indicate that the geometric effect sets in at the fixed radius $3R_*$. Expansion to a radius of $3R_*$ decreases the ratio of diffusion time to dynamical time by only a factor of about ~ 9 relative to its planar value. One has only to move to a slightly ($\sim 30\%$) lower velocity to recover this factor between the two timescales. Therefore, geometrical expansion ends adiabatic acceleration before radiation diffusion ever becomes important—except for the material caught in or very near the shock front at the

moment of emergence. (See Chevalier 1992 for an analysis of a diffusion wave in spherical free expansion.)

So, we are justified in applying the full, adiabatic, planar acceleration factor $(v_f/v_s)_p$ to the shock velocity at breakout in order to estimate the upper velocity limit $v_{f\,\max}$ for which adiabatic results hold.

For convective ($n = 3/2$) and radiative ($n = 3$) envelopes of typical RSG and BSG dimensions, respectively, we find

$$v_{f\max} = 13{,}000\left(\frac{\kappa}{0.34\ \mathrm{cm^2\ g^{-1}}}\right)^{0.13}\left(\frac{\rho_1}{\rho_*}\right)^{-0.086} \times \left(\frac{E_{\rm in}}{10^{51}\ \mathrm{ergs}}\right)^{0.57}\left(\frac{M_{\rm ej}}{10\ M_\odot}\right)^{-0.44} \times \left(\frac{R_*}{500\ R_\odot}\right)^{-0.26}\ \mathrm{km\ s^{-1}}\quad \left(n=\frac{3}{2}\right), \quad (32)$$

$$v_{f\max} = 33{,}000\left(\frac{\kappa}{0.34\ \mathrm{cm^2\ g^{-1}}}\right)^{0.16}\left(\frac{\rho_1}{\rho_*}\right)^{-0.054} \times \left(\frac{E_{\rm in}}{10^{51}\ \mathrm{ergs}}\right)^{0.58}\left(\frac{M_{\rm ej}}{10\ M_\odot}\right)^{-0.42} \times \left(\frac{R_*}{50\ R_\odot}\right)^{-0.32}\ \mathrm{km\ s^{-1}}\quad (n=3)\,.$$

Note the insensitivity of $v_{f\max}$ to the structure parameter ρ_1/ρ_*.

5.3.2. *Relativistic Mass Ejection*

Recently, Kulkarni et al. (1998) have inferred that the radio-bright shell around the peculiar SN 1998bw expanded relativistically during the period of observation, and they take this to be physical evidence of the possible association (Soffita et al. 1998) with the gamma-ray burst GRB 9804025. Woosley, Eastman, & Schmidt (1998) considered models for 1998bw with ejected masses in the range 5–12 $M_\odot$ and energies in the range 4–30 $\times$ 10^{51} ergs. We are motivated by these developments to reconsider the question of relativistic mass ejection, addressed initially by Colgate & Johnson (1960) and Colgate & White (1966) and most recently by Woosley et al. (1998).

Our criterion for relativistic mass ejection is that the maximum ejecta velocity given by our nonrelativistic theory, equation (32), exceed the speed of light. (For the behavior of shock waves in the relativistic regime, see Colgate & Johnson 1960; Johnson & McKee 1971). The star must be sufficiently compact to meet this criterion. For instance, applying equation (32) to an explosion of 10^{51} ergs in a white dwarf, $v_{f\max}$ would be of order $1.7c$ if $n = 3/2$, climbing to $\sim 5.4c$ if $n = 3.25$ in the atmosphere. However, the helium star progenitors of ordinary Type Ib and Ic supernovae may not be compact enough. Taking stellar and ejected masses for such progenitors as considered by Woosley, Langer, & Weaver (1995), and using their radii at carbon ignition (1–9 $R_\odot$) and an effective outer polytropic index $n_{\rm eff} = 3$ to represent the presupernova star, explosions of 10^{51} ergs produce maximum final velocities in the range $0.5c$–$0.7c$.

In the periphery of a star, the shock velocity is a simple power law of initial density (eq. [17]), with the coefficient given by equation (18). In order for the nonrelativistic extrapolation of the final velocity of a mass shell to exceed c, its initial density must be smaller than the mean density by a critical factor: taking $\beta_1 = 0.19$ and $v_f/v_s = 2.1$ in equation (17),

$$\rho_0 \lesssim \left(\frac{1.7v_*}{c}\right)^{5.3}\rho_*\,. \quad (33)$$

However, the electron-scattering optical depth of this material must exceed about 2 or the radiation driving the shock will escape. For an outer density law $\rho_0 = \rho_1(1 - r_0/R_*)^n$, this criterion puts an upper bound on the radius:

$$R_* \lesssim 10^{13.9-2.4/n}\left[\frac{\kappa/0.34\ \mathrm{cm^2\ g^{-1}}}{(1+n)(\rho_1/\rho_*)^{1/n}}\right]^{1/2} \times \left(\frac{E_{\rm in}}{10^{52}\ \mathrm{ergs}}\right)^{1.3(1+1/n)}\left(\frac{M_{\rm ej}}{1\ M_\odot}\right)^{1/2-1.3(1+1/n)}\mathrm{cm}\,. \quad (34)$$

If the star is sufficiently compact by the above criterion, equations (9) and (24) give a rough estimate for the mass of relativistic ejecta:

$$M_{\rm rel} \sim \frac{10^{29.6-4.8/n}}{n+1}\left(\frac{\rho_1}{\rho_*}\right)^{-1/n}\left(\frac{E_{\rm in}}{10^{52}\ \mathrm{ergs}}\right)^{2.6(1+1/n)} \times \left(\frac{M_{\rm ej}}{1\ M_\odot}\right)^{1-2.6(1+1/n)}\mathrm{g}\,. \quad (35)$$

We have assumed that the initial depth of this material is small compared to R_*. An explosion of 10^{52} ergs ejecting $1M_\odot$ in a sufficiently compact star (with $n = 3$ or, as considered by Colgate & Johnson 1960, $n = 3.25$) will produce relativistic ejecta with $M_{\rm rel}c^2 \simeq 3 \times 10^{48}$ ergs, for typical values of ρ_1/ρ_*. (However, to compare, we would predict a shock velocity 50% higher than Colgate & Johnson found, at the point where $\rho_0 = 30\ \mathrm{g\ cm^{-3}}$ in their progenitor.) This energy is comparable to the minimum energy associated with relativistic electrons in SN 1998bw (10^{49} ergs; Kulkarni et al. 1998) and greater than the energy in the gamma-ray burst (8.5×10^{47} ergs; Galama et al. 1998), if the burst and supernova are associated.

5.3.3. *Observable Aspects of Shock Emergence*

The shock velocity approximation of § 4 allows us to predict the variation of the breakout quantities with the explosion parameters $E_{\rm in}$, R_*, M_*, and ρ_1/ρ_*. The quantities that can be extracted from simple analytic calculations include the postshock radiation temperature $T_{\rm se}$, the outburst energy $E_{\rm se}$, and the timescale on which radiation diffuses out of the shock, $t_{\rm se}$ (assuming nonrelativistic ejection). Detailed information about shock emergence, such as the hydrodynamics of optically thin material (which has been suggested to form a thin, dense shell; see, e.g., Ensman & Burrows 1992) or the spectrum of the outburst, are beyond the scope of our simple analysis. The outburst spectrum is affected by the work that photons do as they diffuse out of the shock; a detailed solution awaits multifrequency radiation hydrodynamics simulations. Nonetheless, the values of $T_{\rm se}$ given below agree with recent estimates of the peak color temperature in outburst (see, e.g., Ensman & Burrows 1992) to within 10%.

The postshock radiation temperature is related to the postshock pressure at the time of shock emergence, so

$aT_{se}^4/3 = 2\rho_0 v_s^2(\text{breakout})/(\gamma+1)$:

$$T_{se} = 5.55\times10^5\left(\frac{\kappa}{0.34\ \text{cm}^2\ \text{g}^{-1}}\right)^{-0.10}\left(\frac{\rho_1}{\rho_*}\right)^{0.070} \times\left(\frac{E_{in}}{10^{51}\ \text{ergs}}\right)^{0.20}\left(\frac{M_{ej}}{10\ M_\odot}\right)^{-0.052} \times\left(\frac{R_*}{500\ R_\odot}\right)^{-0.54}\ \text{K}\quad\left(n=\frac{3}{2}\right), \tag{36}$$

$$T_{se} = 1.31\times10^6\left(\frac{\kappa}{0.34\ \text{cm}^2\ \text{g}^{-1}}\right)^{-0.14}\left(\frac{\rho_1}{\rho_*}\right)^{0.046} \times\left(\frac{E_{in}}{10^{51}\ \text{ergs}}\right)^{0.18}\left(\frac{M_{ej}}{10\ M_\odot}\right)^{-0.068} \times\left(\frac{R_*}{50\ R_\odot}\right)^{-0.48}\ \text{K}\quad(n=3)\,.$$

The energy E_{se} of the radiation outburst can be estimated as the thermal energy in the shock front at the time of breakout. So, $E_{se}\simeq(aT_{se}^4/3)[4\pi R_*^3\,x_0(\text{breakout})]$:

$$E_{se} = 1.7\times10^{48}\left(\frac{\kappa}{0.34\ \text{cm}^2\ \text{g}^{-1}}\right)^{-0.87}\left(\frac{\rho_1}{\rho_*}\right)^{-0.086} \times\left(\frac{E_{in}}{10^{51}\ \text{ergs}}\right)^{0.56}\left(\frac{M_{ej}}{10\ M_\odot}\right)^{-0.44} \times\left(\frac{R_*}{500\ R_\odot}\right)^{1.74}\ \text{ergs}\quad\left(n=\frac{3}{2}\right), \tag{37}$$

$$E_{se} = 7.6\times10^{46}\left(\frac{\kappa}{0.34\ \text{cm}^2\ \text{g}^{-1}}\right)^{-0.84}\left(\frac{\rho_1}{\rho_*}\right)^{-0.054} \times\left(\frac{E_{in}}{10^{51}\ \text{ergs}}\right)^{0.58}\left(\frac{M_{ej}}{10\ M_\odot}\right)^{-0.42} \times\left(\frac{R_*}{50\ R_\odot}\right)^{1.68}\ \text{ergs}\quad(n=3)\,.$$

The energy E_{se} will be released on the diffusion time at shock breakout, which is also the time for the shock to travel its width. So,

$$t_{se} = 790\left(\frac{\kappa}{0.34\ \text{cm}^2\ \text{g}^{-1}}\right)^{-0.58}\left(\frac{\rho_1}{\rho_*}\right)^{-0.28} \times\left(\frac{E_{in}}{10^{51}\ \text{ergs}}\right)^{-0.79}\left(\frac{M_{ej}}{10\ M_\odot}\right)^{0.21} \times\left(\frac{R_*}{500\ R_\odot}\right)^{2.16}\ \text{s}\quad\left(n=\frac{3}{2}\right), \tag{38}$$

$$t_{se} = 40\left(\frac{\kappa}{0.34\ \text{cm}^2\ \text{g}^{-1}}\right)^{-0.45}\left(\frac{\rho_1}{\rho_*}\right)^{-0.18} \times\left(\frac{E_{in}}{10^{51}\ \text{ergs}}\right)^{-0.72}\left(\frac{M_{ej}}{10\ M_\odot}\right)^{0.27} \times\left(\frac{R_*}{50\ R_\odot}\right)^{1.90}\ \text{s}\quad(n=3)\,.$$

However, note that the pulse will be longer than this from the vantage of a distant observer because of the light travel time (see, e.g., Ensman & Burrows 1992), which is 1160 s for a star of radius 500 $R_\odot$, or 116 s for a star of radius 50 $R_\odot$. As a result, the observed luminosity will be typically somewhat less than E_{se}/t_{se}.

These formulae reproduce the energy and timescale of the radiation outburst in the numerical simulations of Ensman & Burrows (1992), for explosion parameters chosen to match theirs. These formulae are also in agreement with the analytical results of Imshennik & Nadëzhin (1989) for SN 1987A, but only if we account for the fact that the shock velocity they use is 47% faster than is given by equation (17) for the same model, as if Γ were 1.16 instead of 0.79 for the outermost mass shells. If instead we use equations (36) and (37), we find a value of T_{se} that is 20% lower, and a value of E_{se} that is 50% lower, than those of Imshennik & Nadëzhin. It is not apparent why the two shock formulae do not agree, as their formula is taken from their simulations, and our formula agrees with our simulations.

For the helium-star progenitors of typical Types Ib and Ic supernovae, described by Woosley et al. (1995) and discussed in § 5.3.2 (again, assuming that $E_{in}=10^{51}$ ergs), the energy associated with the outburst would be between 3×10^{44} and 2×10^{46} ergs, and the outburst would last between 2 and 20 s. In making these estimates, we have assumed that the stellar wind does not have sufficient optical depth to support a radiation-dominated shock. For compact progenitors with dense Wolf-Rayet winds, this assumption may fail. In that situation, the shock-velocity formula (eq. [17]) can be applied to the stellar wind, and breakout quantities can be estimated at the radius for which the wind optical depth matches $\sim c/v_s$. The circumstellar interaction (see, e.g., Fransson, Lundqvist, & Chevalier 1996) would then begin immediately.

6. PRESSURE-BASED MODEL FOR THE EJECTA PRESSURE AND DENSITY DISTRIBUTIONS

We now wish to present a model that describes the distribution of all the ejecta, not just the high-velocity ejecta discussed in § 5. To do so, we will extend the form of the pressure distribution inward in mass, approximating its variation with a simple functional form. In our calculations, the final pressure distribution is invariably the smoothest of the hydrodynamical variables (expressed as functions of $\tilde{m}$); this is not surprising, since the pressure gradient is inhibited on small scales by its ability to accelerate the material so as to reduce its magnitude. Once we make a model for the final pressure distribution, the final density distribution follows immediately from the entropy left behind by the forward shock.

To make a simple model for the final pressure distribution, $p_f(\tilde{m})t^4$, we multiply the pressure distribution known for the high-velocity material, given in Table 3, by a simple function of m. This has the advantage of preserving the high-velocity behavior of the flow derived in § 5, because $\tilde{m}$ varies very little in the region of validity of this solution. The solution found in this manner is less accurate than the solutions of § 5, but they have the advantage that they are robust to variations in the progenitor structure (like the existence of superadiabatic gradients in RSGs). They fail in regions that experience a strong reverse shock, especially the mantles of RSGs. However, as we discuss in § 6.1, the density jump between the mantle and outer envelope ejecta *can* be predicted despite the formation of reverse shocks.

Multiplying the pressure distribution specified in Table 3 by a simple function of mass produces our model for the

final radiation pressure distribution:

$$\frac{p_f(\tilde{m})t^4}{p_* t_*^4} = \left[\frac{p_f(\tilde{m})t^4}{p_* t_*^4}\right]_{\rm PL+HV} [1 - \alpha(1 - \tilde{m})]^{4/3} , \quad (39)$$

where $[p_f(\tilde{m})t^4/p_* t_*^4]_{\rm PL+HV}$ is the pressure distribution given in Table 3, that is, a self-similar outer power law times a correction factor that accounts for the geometrical effects spherical expansion. The new term, $[1 - \alpha(1 - \tilde{m})]^{4/3}$, is but another correction factor that accounts for our imperfect knowledge of the pressure distribution in the bulk of the ejecta; we have chosen the power 4/3 to simplify the result for the final density distribution. It remains only to specify the free parameter α used in equations (39), (41), and (42). In § 8 we will develop a technique for generating realistic RSG progenitors with which to constrain α; the variation of α with the stellar structure parameters of red supergiants is presented in Table 4.

The final density distribution corresponding to the ejecta pressure model of equation (39) is obtained by means of the entropy deposited in the forward shock,

$$\frac{\rho_f(\tilde{m})t^3}{\rho_* t_*^3} = \left[\frac{p_f(\tilde{m})t^4}{p_* t_*^4}\right]^{1/\gamma}\left[\frac{s(\tilde{m})}{s_*}\right]^{-1} , \quad (40)$$

where $s(\tilde{m})$ is given by equation (20). Writing out the resulting density model in terms of the variables $\tilde{m}$, r_0, and ρ_0, we find

$$\frac{\rho_f(\tilde{m})t^3}{\rho_* t_*^3} = \Lambda_\rho(1 - \tilde{m})^{3w_p/4}\tilde{m}^{(3-6\beta_1)/4}\left(\frac{r_0}{R_*}\right)^{9\beta_1/2}\left(\frac{\rho_0}{\rho_*}\right)^{(1+6\beta_1)/4}$$
$$\times [1 - \alpha(1 - \tilde{m})]\begin{cases}(1 + 0.96\,\delta\tilde{m})^{3/4} & (n = 3/2) ,\\ (1 + 1.03\,\delta\tilde{m} + 0.37\,\delta\tilde{m}^2)^{3/4} & (n = 3) .\end{cases} \quad (41)$$

The only parameter remaining to be determined is the numerical prefactor Λ_ρ. The planar, self-similar solution gives the definite value $\Lambda_\rho = 11 f_p(1)^{3/4}$, where $f_p(1)$ is given by equation (22). However, we find that using overall energy conservation to set Λ_ρ gives more accurate results. To do this, we first derive the velocity distribution from the density model by means of a numerical integration:

$$\frac{v_f(\tilde{m})^3}{v_*^3} = \frac{3}{4\pi}\int_0^{\tilde{m}}\left[\frac{\rho_f(\tilde{m}')t^3}{\rho_* t_*^3}\right]^{-1} d\tilde{m}' . \quad (42)$$

(Note that by integrating from zero velocity, we have excluded the remote possibility of hollow blastwaves, which can occur in special distributions; see Ostriker & McKee 1988.) If we define the model energy $E_{\rm model}$ by

$$\frac{E_{\rm model}}{E_{\rm in}} \equiv \frac{1}{2}\int_0^1 \frac{v_f(\tilde{m})^2}{v_*^2}\, d\tilde{m}' , \quad (43)$$

then the energy of the ejecta model can be brought into agreement with $E_{\rm in}$ by the transformation (from eq. [1])

$$\frac{v_f(\tilde{m})}{v_*} \to \frac{v_f(\tilde{m})}{v_*}\left(\frac{E_{\rm model}}{E_{\rm in}}\right)^{-1/2} ,$$
$$\frac{\rho_f(\tilde{m})t^3}{\rho_* t_*^3} \to \frac{\rho_f(\tilde{m})t^3}{\rho_* t_*^3}\left(\frac{E_{\rm model}}{E_{\rm in}}\right)^{3/2} , \quad (44)$$
$$\frac{p_f(\tilde{m})t^4}{\rho_* t_*^4} \to \frac{p_f(\tilde{m})t^4}{\rho_* t_*^4}\left(\frac{E_{\rm model}}{E_{\rm in}}\right)^{2} .$$

In this transformation, the characteristic scales (v_*, etc.) are kept fixed but the model ejecta distributions [$v_f(\tilde{m})$, etc.] are altered to agree with the blastwave energy.

Equation (41) constitutes a local model for the final ejecta distribution, one that specifies the final density of a mass shell by reference to its initial variables (m, r_0, ρ_0) only. The enforcement of overall energy conservation and the application of the parameter α weaken this statement only slightly. This model inherits from the entropy and shock-velocity models its inability to describe regions that have been hit by strong reverse shocks. An underestimate of the entropy leads to an overestimate of the density in the mantles of supergiants, especially RSGs.

6.1. *Density Variation across the Outer Composition Boundary*

Independently of our model for the distribution of the outer envelope ejecta, our shock-velocity model allows us to evaluate the relative jump in density at the base of the outer envelope. This boundary is typically the outermost composition boundary in the progenitor. If we take $p_f(\tilde{m})t^4$ to be continuous in $\tilde{m}$ across the boundary, the entropy left behind by the shock wave, equation (41) with $\beta_1 = 0.19$, dictates

$$\delta \log (\rho_f t^3) = 0.54\delta \log (\rho_0) + 0.86\delta \log (r_0) , \quad (45)$$

where $\delta \log (\rho_0)$ and $\delta \log (r_0)$ are to be evaluated for nearby mass shells straddling the composition boundary.

One might be concerned that this result would be invalidated by the formation of a reverse shock at this boundary,

TABLE 4

PARAMETERS FOR MODELING THE H EJECTA FROM RSGs

Parameter	Value
Typical RSG Sequence (eq. [48])	
α	$5.58q^2 - 0.10q - 1.17$
$\rho_{\rm break} t^3/\rho_* t_*^3$	$10^{-3}(5.21q^2 - 10.12q + 5.40)$
$v_{\rho_{\rm break}}/v_*$	$0.93q + 1.94$
$l_{\rho 1}$	$-3.06q^2 + 2.03q - 0.46$
$l_{\rho 2}$	-11.731
y_ρ	4.5
$p_{\rm break} t^4/p_* t_*^4$	$10^{-4}(-9.87q^2 + 4.67q + 4.87)$
$v_{p_{\rm break}}/v_*$	$0.80q + 1.85$
l_{p1}	$1.68q - 1.89$
l_{p2}	-11.895
y_p	3.8
Partial Derivatives, for Extrapolation	
$\partial\alpha/\partial(M_{\rm env}/M_{\rm ej})$	$-17.9q + 3.67$
$\partial(\rho_{\rm break} t^3/\rho_* t_*^3)/\partial(M_{\rm env}/M_{\rm ej})$	$10^{-3}(-10.12q + 9.53)$
$\partial(v_{\rho_{\rm break}}/v_*)/\partial(M_{\rm env}/M_{\rm ej})$	$1.14q - 1.43$
$\partial l_{\rho 1}/\partial(M_{\rm env}/M_{\rm ej})$	$3.82q - 1.38$
$\partial(p_{\rm break} t^4/p_* t_*^4)/\partial(M_{\rm env}/M_{\rm ej})$	$10^{-3}(1.53q - 0.43)$
$\partial(v_{p_{\rm break}}/v_*)/\partial(M_{\rm env}/M_{\rm ej})$	$0.28q - 0.81$
$\partial l_{p1}/\partial(M_{\rm env}/M_{\rm ej})$	$-0.74q - 2.13$

NOTE.—The parameters used in eqs. (46) and (47) specify the harmonic-mean approximation for the hydrogen ejecta of red supergiants described in § 7; in eq. (41), α specifies the more complicated pressure-based model of § 6. Parameters that depend on q are derived from the one-parameter family of progenitors described by eq. (48) and shown as the dashed line in Fig. 5. Partial derivatives corresponding to changing the remnant mass without changing M_* or $M_{\rm env}$ (i.e., at fixed q) are derived from comparison with a second sequence of models offset by 0.05 in $M_{\rm env}/M_{\rm ej}$. The fit for α is valid in the range $0.3 \le q \le 0.6$; others are valid for $0.3 \le q \le 0.8$.

TABLE 5

FIDUCIAL EJECTA MODELS FOR RADIATIVE PROGENITORS

Parameter	Value	Comments
α	0	Typical value
$\rho_{\rm break} t^3/\rho_* t_*^3$	1.91×10^{-3}	Energy and mass conservation
$v_{\rho\ {\rm break}}/v_*$	2.30	Energy and mass conservation
$l_{\rho\ 1}$	-1.06	Theory of Chevalier & Soker 1989
$l_{\rho\ 2}$	-10.176	Self-similar value ($n = 3$)
y_ρ	~ 4.5	From RSG models
$p_{\rm break} t^4/p_* t_*^4$	$\sim 2.4 \times 10^{-4}$	Gleaned from simulation
$v_{p\ {\rm break}}/v_*$	~ 2.3	From RSG models
$l_{p\ 1}$	2.22	Theory of Chevalier & Soker 1989
$l_{p\ 2}$	-9.77	Self-similar value ($n = 3$)
y_p	3.8	From RSG models

NOTE.—Parameters for modeling the entire ejecta of radiative stars. Without a sequence of reliable models to fit, these models are only educated guesses. The harmonic-mean model (all but α) is a combination of the self-similar rarefaction hypothesis of Chevalier & Soker 1989 with self-similar planar expansion for $n = 3$ and softening parameters y_ρ, y_p taken from the RSG fits. We simply assume $\alpha = 0$ to specify a pressure-based model. The pressure-based model reflects the detailed progenitor structure through the entropy deposited in the shock, whereas the harmonic-mean model is inflexible. Note that the effect of the reverse shock is less severe for these progenitors than for RSGs, so the mantle is better represented.

or by the development of the Rayleigh-Taylor instability. However, in our simulations the compression wave that decelerates the mantle material travels inward (in mass) before it steepens into a shock wave, so that the entropy distribution given by equation (20) is correct across the boundary. The Rayleigh-Taylor instability may indeed break the spherical symmetry of the ejecta. However, it is unlikely to change the fact that the outermost mantle ejecta is in contact with the innermost ejecta of the outer envelope. Then, pressure equilibrium across the boundary gives the density jump above. An interesting corollary is that the temperature distribution is continuous as well, even once radiation diffusion becomes significant. This may have implications for the recombination epoch, since helium (with a much lower specific entropy) underlies any hydrogen-rich ejecta.

Those interested in modeling the distribution and expansion velocity of the radioactive inner mantle material should note that our model for the outer envelope ejecta constrains these quantities rather poorly, because we overestimate the density of the mantle material.

7. HARMONIC MEAN MODELS FOR EJECTA DISTRIBUTIONS

Our simulations demonstrate that the final density and pressure in the hydrogen ejecta can often be fit reasonably by the simple density model

$$\frac{\rho_f t^3}{\rho_* t_*^3} = \frac{\rho_{\rm break} t^3}{\rho_* t_*^3} \times \left[\frac{(v_f/v_{\rho{\rm break}})^{-l_{\rho 1}/y_\rho} + (v_f/v_{\rho{\rm break}})^{-l_{\rho 2}/y_\rho}}{2} \right]^{-y_\rho} \quad (46)$$

and the corresponding pressure model

$$\frac{p_f t^4}{p_* t_*^4} = \frac{p_{\rm break} t^4}{p_* t_*^4} \times \left[\frac{(v_f/v_{p{\rm break}})^{-l_{p1}/y_p} + (v_f/v_{p{\rm break}})^{-l_{p2}/y_p}}{2} \right]^{-y_p} . \quad (47)$$

These models interpolate between limiting power laws at low and high velocities, joined at a specified value ($\rho_{\rm break}$ or $p_{\rm break}$) at a given break velocity ($v_{\rho{\rm break}}$ or $v_{p{\rm break}}$), with a curvature set by the parameters y_ρ or y_p.

For supernovae in red supergiants, these models apply only to the hydrogen ejecta, because of the severe density

TABLE 6

CALIBRATION OF EJECTA MODELS FOR REALISTIC PROGENITORS

	RSG[a]		BSG[b]	
ERROR ESTIMATE	H envelope	Mantle	H envelope	Mantle
Pressure-based Model (§ 6)				
$\langle \delta\rho_f/\rho_f \rangle_{\tilde m}$	0.07	6.1	0.10	0.71
$[\delta\rho_f(\tilde m)/\rho_f(\tilde m)]_{\rm max}$	2.1	21	7.5	5.8
$\langle \delta\rho_f/\rho_f \rangle_{\log(v_f)}$	0.34	4.5	0.96	3.0
$[\delta\rho_f(v_f)/\rho_f(v_f)]_{\rm max}$	1.4	32	4.5	15
Harmonic-Mean Model (§ 7)				
$\langle \delta\rho_f/\rho_f \rangle_{\tilde m}$	0.20	...	0.31	0.70
$[\delta\rho_f(\tilde m)/\rho_f(\tilde m)]_{\rm max}$	4.5	...	0.83	22
$\langle \delta\rho_f/\rho_f \rangle_{\log(v_f)}$	1.5	5.0	0.53	3.2
$[\delta\rho_f(v_f)/\rho_f(v_f)]_{\rm max}$	10	18	2.4	19

NOTE.—Mean and maximum relative errors in the density models of this paper, for both the Lagrangian and Eulerian functions $\rho_f(m)t^3$ and $\rho_f(v_f)t^3$. Mean errors are computed according to the formula $\langle \delta\rho_f/\rho_f \rangle_x \equiv \exp(\langle \{\log[\rho_{\rm model}(x)/\rho_f(x)]\}^2 \rangle_x)^{1/2} - 1$, where $\langle\rangle_x$ is a mean weighted evenly in the variable x. The maximum error is defined consistently: an error of 1 implies a factor of 2 (in either direction) between $\rho_f(x)t^3$ and $\rho_{\rm model}(x)t^3$. In RSGs, the harmonic mean approximation does not cover the mantle. Errors in the H envelope are dominated by variations in the effective polytropic index from its ideal value (3/2 for RSGs and 3 for BSGs) in the outer layers of the progenitor. Errors in the mantle are dominated by the effect of the reverse shock, which is not addressed in these models.

[a] 15 $M_\odot$ RSG of Woosley & Weaver 1995, courtesy of Stan Woosley

[b] 16 $M_\odot$ BSG of Shigeyama & Nomoto 1990, courtesy of Ken'ichi Nomoto.

jump at the base of this material. As a result, we cannot apply the constraints of mass and energy conservation to give relations between the five parameters $\rho_b t^3$, $v_{\rho\text{break}}$, $l_{\rho 1}$, $l_{\rho 2}$, and y_ρ in the density model. Instead, we fix $l_{\rho 2}$ and l_{p2} at their self-similar values; we set y_ρ and y_p at characteristic values; and we fit the other three as functions of q, using the techniques in § 8. Table 4 presents these fits for red supergiants.

These simple models fit the outer envelope ejecta of polytropic models for red supergiants quite accurately, to about 9%–11% error in density and 23%–30% error in pressure (both errors increasing with increasing q). In fact, the residuals have a very consistent pattern in each case, indicating that more complicated models could achieve even greater accuracy. However, real stars may not resemble polytropes sufficiently to justify any more complexity.

For supernovae in stars with radiative outer envelopes, such as blue supergiants, no sequence of simple models is available for the fitting of these parameters. However, the difference between mantle and outer envelope is not as severe for these stars, so we can apply models to the entire ejecta at once. The constraints of mass and energy conservation then reduce the number of parameters in the density model from five to three. The outer power-law behavior is strongly constrained by the planar, self-similar solution. Chevalier & Soker (1989) conjectured that the interior power law could be described by self-similar rarefaction, a hypothesis we also adopt to set $l_{\rho 1}$ and l_{p1}. Taking y_ρ to be the same as in the RSG models, the density distribution is fully specified. For the parameters y_p, $v_{p\text{break}}$ and p_{break} of the model pressure, few constraints are available. We quote typical values only. The result is a fiducial model, given in Table 5, that may be representative, but which depends not at all on the actual progenitor structure. In this sense, the pressure-based model of § 6 is superior, especially for radiative progenitors. See Table 6 for a synopsis of the relative accuracy of these models for realistic blue and red supergiant progenitors.

8. SURVEY OF EJECTA DISTRIBUTIONS FROM MODEL RED SUPERGIANTS

The extreme difference in density between the mantles and outer envelopes of red supergiants, as well as the relative constancy of the hydrogen envelope density, suggest that simple models can reproduce the dynamics and final density distribution of these stars. Such an approach was taken by Chevalier (1976), who found that progenitor models with constant-density mantles and constant-density outer envelopes, separated by a region of steep density decline, could reproduce the qualitative features of Type II light curves. Most notably, he identified existence of a plateau phase with the formation of a "detached shell" (density maximum) in the final distribution. We will use a different set of simplified models to represent these progenitors, so it is worthwhile to review in detail why such models are realistic.

In red supergiants, the outer convective envelope can be modeled as a polytrope of index $n = 3/2$ (§ 3), so that the shape of its density distribution is determined by the ratio of its mass to that of the star, $q = 1 - M_{\text{env}}/M_{\text{ej}}$. Clearly, the initial distribution of density in the progenitor will affect the final distribution of density in the ejecta.

There is one other parameter that plays an important role in determining the ejecta distributions from the convective outer envelopes of red supergiants: $M_{\text{env}}/M_{\text{ej}}$, the ratio of the outer envelope's mass to the total ejected mass. This ratio determines how much material (beneath the outer envelope) participates in the explosion. Although the outer envelope will wind up with the lion's share of the final kinetic energy, the mass of underlying ejected mantle is important in the blastwave stage. At the beginning of this phase, the explosion energy is contained within the mantle. During the course of the blastwave, as the explosion energy gets transferred to the outer envelope, the mass of the swept-up mantle material continues to affect the forward shock velocity (eq. [17]).

Note that the shock velocity in the outer envelope (as approximated by eq. [4]) is affected by the mass of the mantle, but not (to the accuracy of this approximation) by its structure. Indeed, there is reason to believe that this property should hold for the final ejecta distribution as well. Our pressure-based model for the ejecta is a local theory, making reference to the initial variables (m, r_0, ρ_0) in the progenitor. The distinction between remnant and mantle affects the mass coordinate m, so the mass ratio $M_{\text{env}}/M_{\text{ej}}$ affects our prediction for the outer envelope ejecta. However, the initial radius and structure of the mantle do not, so we are justified in using simplified models whose mantles have realistic masses but idealized structures.

The two parameters $q = 1 - M_{\text{env}}/M_*$ and $M_{\text{env}}/M_{\text{ej}}$ are clearly correlated for real progenitors, because M_* and M_{ej} differ by only the remnant mass M_{rem}. Indeed, only certain values of these two parameters are realistic, as depicted by Figure 5. Although the loss of the outer envelope mass in isolated stars and binaries is uncertain and intrinsically variable, the evolution of stellar cores and mantles appears to be nearly independent of mass loss and initial metallicity while a hydrogen envelope persists (Woosley & Weaver

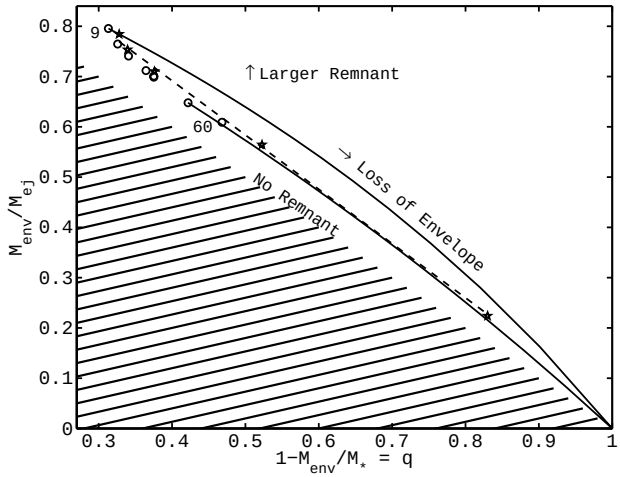

FIG. 5.—Mass ratios that parameterize Type II supernovae. Plotted is the envelope fraction in the ejecta vs. the ratio q of core to stellar mass. If remnant masses are correctly estimated, progenitors must lie in the swath between the solid lines regardless of mass loss. As a star loses its envelope, it travels from the point corresponding to no mass loss (*circles*; from Maeder 1992 for 9, 12, 20, 25, 40, and 60 $M_\odot$) along a curve (*solid lines*; for 9 and 40 $M_\odot$) toward the point (1, 0). The results of lone stellar mass loss at solar metallicity (*stars*; Woosley & Weaver 1995) for 9, 12, 20, and 25 $M_\odot$ lie in the interior. Stars initially above about 27 $M_\odot$ will retain their envelopes only if the metallicity is low. The remnant mass cannot be negative (*hatched region*), but it could be zero in a thermonuclear explosion. Also shown (*Dashed line*) the sequence of models (eq. [48]) considered in § 8.

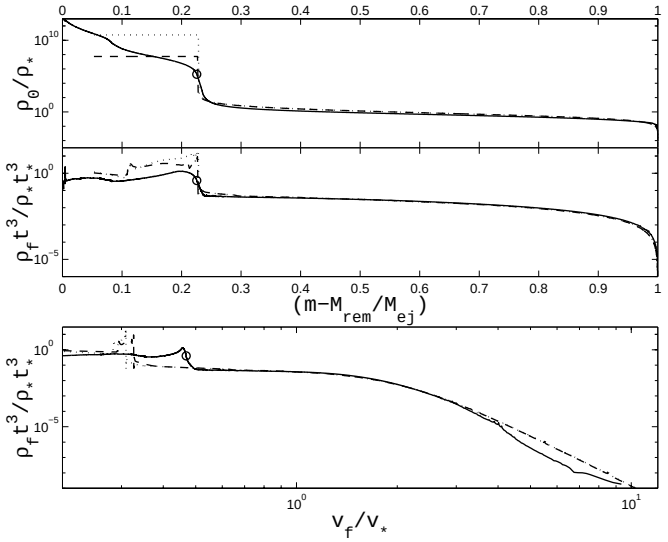

FIG. 6.—Applicability of polytropic models to red supergiant envelopes and the insensitivity of the outer envelope ejecta to the size and structure of the mantle. The red supergiant model of Woosley & Weaver (1995; *solid lines*) has a mantle radius $R_{man} \simeq 0.02R_*$ and a complicated mantle structure resembling $\rho_0 \propto r^{-3}$. The polytropic models have mantles of constant density, with $R_{man} = 10^{-3}R_*$ (*dashed lines*) and $R_{man} = 10^{-4}R_*$ (*dotted lines*). Nevertheless, the outer envelope ejecta is well modeled by both progenitors. The superadiabatic gradient is significant in the subsurface layer of the progenitor, which produces a high-velocity density distribution that differs from polytropic models.

1995; Maeder 1992). Assuming that the fiducial estimate of the remnant mass is correct, this implies that M_{rem} and M_{man} are well known as a function of initial stellar mass. The final value of the hydrogen envelope mass M_{env} depends on uncertain mass loss, but it is unlikely that the final stellar mass M_* of an RSG will exceed the initial main-sequence mass, except perhaps in some massive binaries. The circles in Figure 5 demonstrate the loci of the two parameters for stars that lose no mass; the stars on this line are the models of Maeder (1992), which also agree with those of Woosley & Weaver (1995) and show no significant variation with metallicity. Varying M_{env} between this maximum amount and zero, a star with a certain ratio M_{rem}/M_{man} will trace out a curve (*dotted lines*) in the space of these parameters. As discussed by Woosley & Weaver (1995), the mass-loss rates of isolated stars increase with metallicity. Their calculated final states of solar-metallicity stars are shown as stars in the figure.

It is evident from this figure that only a narrow swath of the parameter space of q and M_{env}/M_{ej} is likely to be inhabited by Type II supernova progenitors, so we are justified in focusing our attention on the one-parameter family (Fig. 5, *dashed line*),

$$\frac{M_{env}}{M_{ej}} = 1.12 - 1.08q\ , \tag{48}$$

for values of q between 0.3 and 0.8. For comparison, we have also considered values of M_{env}/M_{ej} greater by 0.05 at a given q, in order to capture the variation of quantities over the physical range.

Our model star has a dense central region that represents the mantle, which has a small radius (typically $10^{-4}R_*$), a uniform density, and the appropriate mass as given by M_{man}/M_{ej}. Above this lies a polytrope of index $n = 3/2$ that represents the stellar envelope; its structure is given by the value of q under consideration. Explosions in these progenitors are then simulated numerically as outlined in § 9, and the results are analyzed to find the variation of the parameter α for the model of § 6 as a function of q.

We base our trust in these models on demonstrations that their outer envelope ejecta are insensitive to the initial mantle distribution and can match the results of more sophisticated progenitor models. In Figure 6, we show that varying the mantle radius (and thus its density) slightly alters the final distribution of mantle material but not the final distribution of the outer envelope material. This figure also shows that our models can match the outer envelope ejecta in the explosion of the 15 $M_\odot$ model of Woosley, implying that large differences in the initial mantle distribution lead to negligible differences in the final outer-envelope ejecta.

9. CALIBRATION OF MODELS AGAINST SIMULATIONS

9.1. *Simulation Technique*

Our simulations are performed with an explicit, second-order, Lagrangian, finite-differencing code, as described by Richtmyer & Morton (1967). Our code was written by Kelly Truelove, modeled after a code by John Holliman, as described in Truelove & McKee (1998). We have modified it slightly for the simulation of supernovae. Our progenitor distributions were kindly supplied by Ken'ichi Nomoto and Stan Woosley and have been interpolated onto finer Lagrangian grids for more accurate dynamical results. For the study of lone polytropic envelopes, we solved the Lane-Emden equation numerically. After finding the solution corresponding to a desired value of q for a given value of the polytropic index n, we sampled the resulting structure at initial radii $r_0(i) \propto i^l$ to generate the ith Lagrangian element. The sampling parameter l was varied to capture the full range of mass, initial density, and initial radius, and to give the fastest convergence for studies in which the number of zones was varied. When investigating the highest velocity ejecta, we were motivated by spherical truncation of self-similar acceleration (see the Appendix) to distribute the Lagrangian zones evenly in the parameter $x_0^{1/3}$. Runs were performed with between 500 and 10,000 zones, depending on the convergence properties and the fidelity desired for a particular result.

Our calculations were performed with a maximum Courant number of 0.5, and with a coefficient of the quadratic artificial viscosity law $c_0^2 = 2.5$. These values were chosen to optimize the energy and entropy conservation, as well as the numerical shock structure. Small spikes in the ejected mantle of the BSG (seen in Fig. 8) are due to features (deviations from smoothness) in the low-resolution progenitor that we interpolated for our simulations; these are not caused by underresolution of the hydrodynamics. Energy was conserved to within 3% in all our runs, with the discrepancy growing during shock propagation and holding steady after breakout. All calculations were carried out until the thermal pressure was 3 orders of magnitude smaller than the kinetic energy density in every zone; at this stage, pressure gradients could safely be ignored. To determine the forward-shock velocity, we compared the entropy distribution with the initial density distribution. This comparison was made before the passage of a reverse shock, for zones that experienced one. A slight loss of entropy conservation

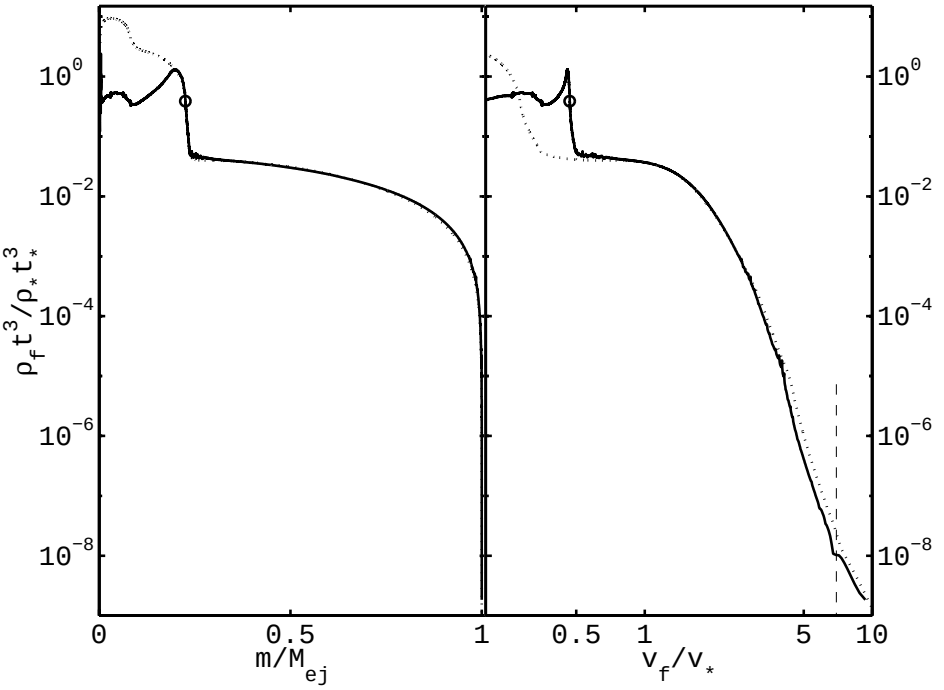

FIG. 7.—Comparison of the pressure-based model (§ 6; *dotted lines*) with the result of simulation for realistic progenitors (*solid lines*, with *circles* at the H-He boundary). The maximum ejecta velocity is marked (§ 5.3; *dashed lines*). Left-hand side: normalized final density $\rho_f t^3/\rho_* t_*^3$ with respect to the normalized ejecta mass $\tilde{m} \equiv m/M_{ej}$. Right-hand side: $\rho_f t^3/\rho_* t_*^3$ vs. the normalized velocity v_f/v_*. The 15 $M_\odot$ red supergiant progenitor model of Woosley & Weaver (1995) was the input into both the simulation and the analytical model. The parameter α was chosen according to the formulae in Tables 4 and 5. Note that the models fail interior to the base of the hydrogen envelope, because of the entropy deposited in the reverse shock, but the jump in density at the base of the outer envelope is correctly estimated (§ 6.1).

(decreasing with increasing resolution) was observed in the range of 10–100 breakout times, and we were careful to record the shock-deposited entropy of all zones by the time of breakout.

9.2. *Comparisons against Simulations of Realistic Progenitors*

We have compared in detail both the pressure-based and the harmonic-mean models for the final density distribution $\rho_f t^3$ against the output of the hydrodynamic code for the case of two progenitor distributions: a 15 $M_\odot$ red supergiant progenitor (Woosley & Weaver 1995, courtesy of S. E. Woosley), and a 16 $M_\odot$ progenitor for SN 1987A (Shigeyama & Nomoto 1990, courtesy of K. Nomoto). The comparison is made graphically in Figures 7, 8, 9, and 10, and the results are summarized in Table 6.

Both models are typically more accurate in the hydrogen envelope of the red supergiant than that of the blue supergiant. This is to be expected, because the parameters of these models were tuned to match the results of simulation using polytropic analogs for convective stars (§ 7). However, the effect of the superadiabatic gradient on the high-velocity ejecta of the RSG is not included in these polytropic analogs. The pressure-based model, which includes more physics, better reflects the initial distribution of this material and incurs only $\sim$34% error [weighted by log (v_f)] as a result. The harmonic-mean model, on the other hand, differs from simulation by about a factor of $\sim$2.5 with the same measure. The difference can also be seen in the figures. This should be considered an error of the polytropic analog, or a demonstration of the effect of the superadiabatic gradient on the high-velocity ejecta.

In the blue supergiant as well, variations of the effective polytropic index dominate the (log velocity–weighted) errors in the high-velocity ejecta. An inspection of the progenitor reveals that $n_{\rm eff}$ approaches and then exceeds 3 in the outer one-half of the radius and then becomes approximately constant in the outermost 10%. The simulation and the models both attain the desired self-similar power-law index at the highest velocities. The deviations away from this index are due to both the effects of sphericity (§ 5.2) and the variation in polytropic index: steeper progenitors (higher $n_{\rm eff}$) give shallower ejecta (lower $l_{\rho 2}$) in self-similar theory (see, e.g., Chevalier & Soker 1989). The pressure-based model does become shallower for lower $n_{\rm eff}$ because of the change in shock velocity, but not as shallow as the true numerical behavior. As a result, an error accumulates because the shape of the ejecta is slightly misrepresented, especially for material that originated in the outer quarter or so of the radius.

It would be possible to expand the analytical description to include variations in $n_{\rm eff}$ from their ideal values of 3/2 and 3 for red and blue supergiants. Such an analysis would be necessary for the association of observational features in the high-velocity ejecta with initial features of the progenitor.

The mantle distribution of the red supergiant is badly represented in both models. The pressure-based model suffers from a gross underestimation of the entropy in this region, because we do not account for the effect of the reverse shock. The harmonic-mean model does not cover the RSG mantle at all, because it was fit only to the outer ejecta in analogous polytropic simulations.

For the blue supergiant, the effect of the reverse shock is not as severe and the pressure-based model fares quite well. Because it is accurate in predicting the density of the mantle ejecta, the velocity of the hydrogen-helium boundary is also

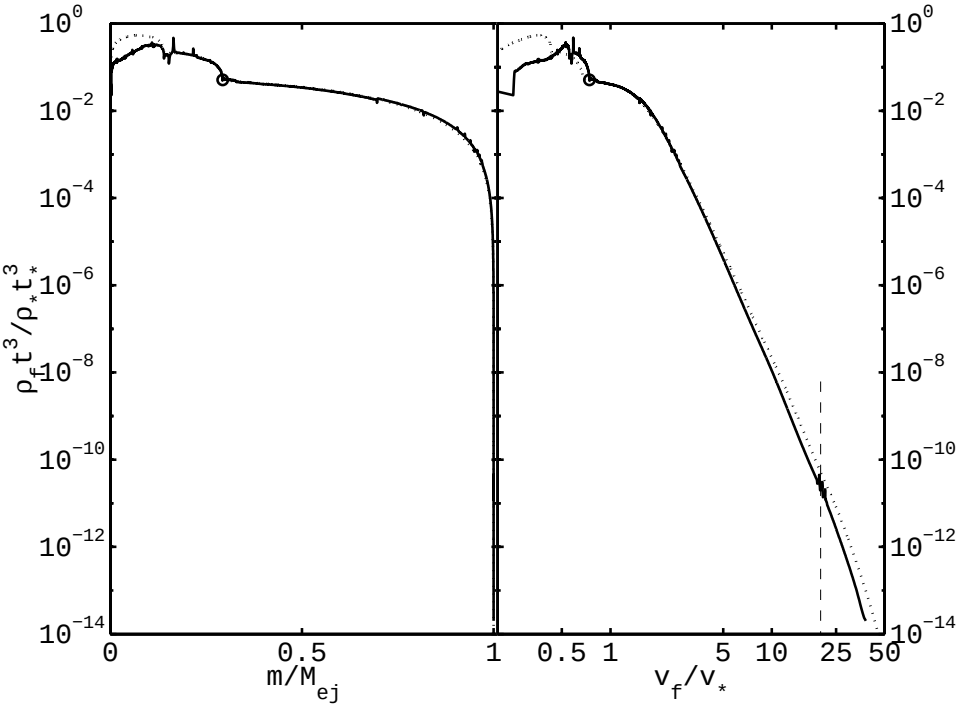

FIG. 8.—Comparison of the pressure-based model with simulation, but here the progenitor was taken to be the 16 $M_\odot$ blue supergiant model of Shigeyama & Nomoto (1990). As in Fig. 7, the solid line is the simulation, with circles at the He-H boundary; the dotted line is the output of the pressure-based model, and a dashed line marks the maximum velocity to which the adiabatic approximation is valid, which is approximately the speed limit for the ejecta. Note the lesser effect of the reverse shock for the BSG compared to the RSG, the higher maximum velocity, and the greater range of ejecta densities. Again, the jump in density at the H-He boundary is correctly determined by the model.

accurately predicted. The harmonic-mean model is aided by the weakness of the reverse shock as well, but this model includes no information about the difference between mantle and outer envelope. As a result, it incurs a significant error in the BSG mantle material.

Note that the pressure-based model correctly predicts the density jump (eq. [45]) between the hydrogen and helium for both red and blue supergiants. The effect of the reverse shock is apparent inward in mass from this jump; it depresses the central density of the red supergiant ejecta,

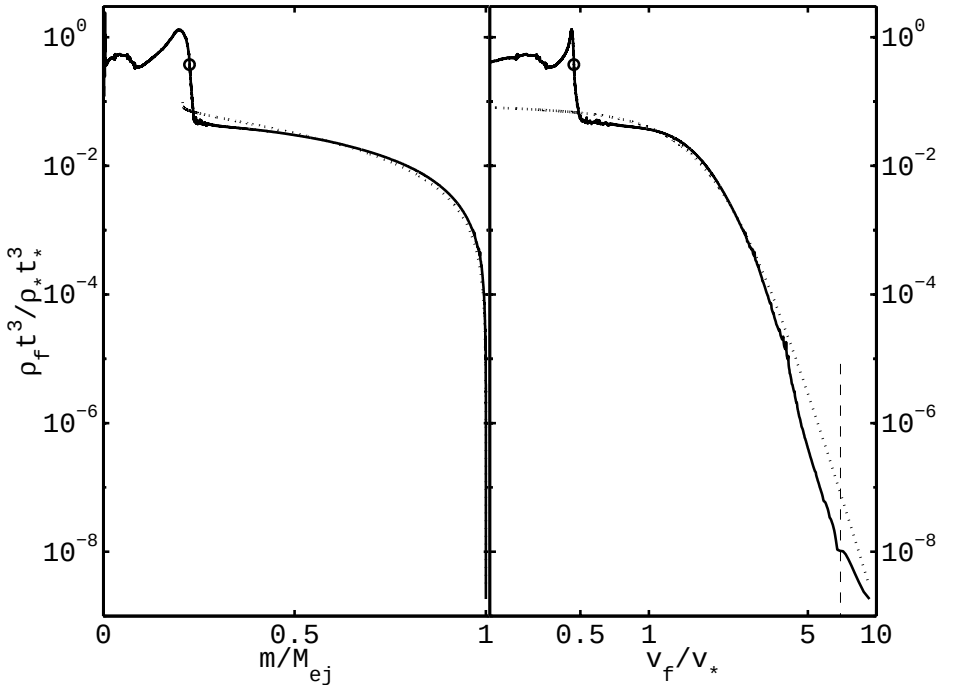

FIG. 9.—Application of the harmonic-mean model (§ 7 and Table 4; *dotted lines*) to the numerical simulation (*solid lines*, with *circles* at the H-He boundary), for the RSG progenitor of Woosley & Weaver (1995). Again, the dashed line shows the maximum velocity of the ejecta. For RSG progenitors, the model is derived from a polytropic progenitor, as tabulated in Table 4. It is meant to describe the hydrogen envelope only. Since the models prescribe $\rho_f(v_f)$, the model mass coordinate is obtained by integrating inward from $\tilde{m} = 1$ at high velocities.

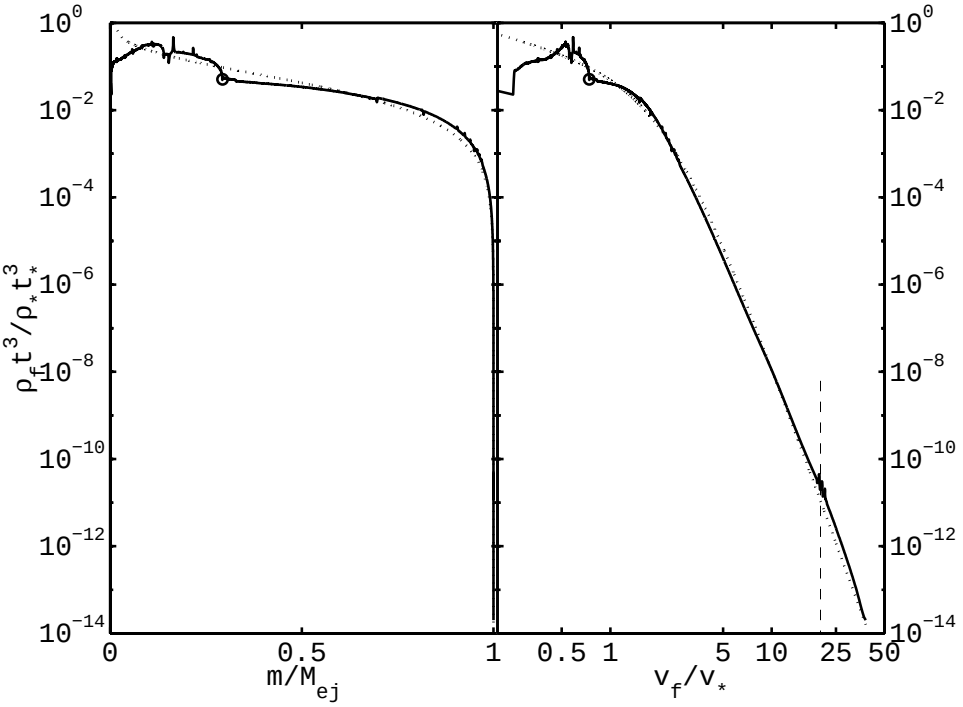

FIG. 10.—Comparison of the harmonic-mean model (§ 7; *dotted lines*) with the simulation (*solid lines*), here for the blue supergiant progenitor of Shigeyama & Nomoto (1990). For the BSG progenitor, the constraints of mass and energy conservation are imposed, and the inner power law is chosen to agree with the self-similar rarefaction model of Chevalier & Soker (1989) (Table 5). This model is therefore meant to cover the entire ejecta distribution.

producing an offset density maximum. We will discuss this phenomenon further in the next section.

Besides the stellar models presented so far, we also investigated the explosion of model 3H11 of Nomoto et al. (1995), provided to us by K. Nomoto. This model, meant to describe the progenitor structure of SN 1993J, has an H envelope of mass 0.11 $M_\odot$, which is very small compared to the 3.4 $M_\odot$ ejected. The envelope's density structure is nonpolytropic; indeed, there is a density minimum at the base of the envelope and a local maximum within it (seen in Fig. 6 of Nomoto et al. 1995). The density then declines toward the surface, but shallows out again, with $d \log \rho / d \log$ depth decreasing from 1 to 0.2. The reverse shock into the He mantle stalls after it has traversed a mass comparable to the envelope mass, leaving behind a jump in density. The shallow initial-density law leads to steeply declining final density in the outermost hydrogen ejecta, as predicted by equation (25) and depicted by Suzuki & Nomoto (1995). The density jump and the variations of outer power law were not reproduced by our pressure-based or harmonic-mean models, although the helium mantle ejecta was fairly well represented.

10. CONCLUSIONS

In this paper we develop analytical approximations that capture the essential elements of spherically symmetric, adiabatic explosions in media of finite mass and extremely stratified density distributions: the progenitors of supernovae. Analytical predictions are motivated and then calibrated by comparison to numerical simulations for realistic red and blue supergiant progenitors. In separate sections we address the velocity law of supernova shock waves (§ 4), the expansion of the highest velocity ejecta (§ 5), and two types of models for the final distribution of ejecta. One of these models (§ 6) specifies the pressure distribution in the ejecta and derives the final density distribution; the other (§ 7) specifies the density directly as a function of final velocity. The benefits and drawbacks of these models, in application to red and blue supergiants, are summarized in Table 1.

We emphasize the structure of the outer (typically hydrogen) envelope ejecta in particular, because this layer is separated from the underlying mantle material by a large drop in initial density. This drop in density leads to an acceleration of the forward shock, followed by a reverse shock into the mantle material as the forward shock decelerates. Although our models can account for the density jump in the ejecta caused by the acceleration of the forward shock (§ 6.1), we make no attempt to model reverse shock propagation, so our models do not describe the mantle material accurately, although this drawback is much less severe for blue supergiants than for red ones.

No doubt the most useful conclusion of this work is that the ejecta distributions from red supergiants are described by the single parameter $q \equiv 1 - M_{\rm env}/M_*$. This simplification occurs because these progenitors follow a sequence in parameter space (the dashed line in Fig. 5) as they lose mass, regardless of the mechanism of stellar mass loss. When these stars explode, their ejected hydrogen envelopes assume a distribution that can be fit reliably by the simple, harmonic-mean models of § 7. The sequence of progenitors produces a sequence of ejecta distributions (with fits tabulated in Table 4). The simplicity of these harmonic-mean models makes them ideal for a systematic analysis of Type II supernova light curves from RSGs. Such an analysis would be useful in calibrating the expanding photospheres method, as discussed by Eastman, Schmidt, & Kirshner (1996).

However, this work is limited by the assumption of strict spherical symmetry in the analytical models and in the numerical simulations against which they are compared. The oblateness of a rotating progenitor (Chevalier & Soker

1989), the instability of accelerating shock waves (albeit slowly growing; Chevalier 1990; Luo & Chevalier 1994), and the Rayleigh-Taylor instability (see, e.g., Herant & Woosley 1994) have interesting effects that are not accounted for here. Moreover, by approximating supernovae as adiabatic, nongravitating point explosions, we have neglected physics that is important for the inner mantle material (where reverse shocks also limit our accuracy).

Our model for the shock velocity (eq. [17]) is the simplest possible formula that combines powers of the local variables m, r_0, and ρ_0 in the progenitor and the blastwave energy $E_{\rm in}$ in a manner consistent with both spherical and planar scaling laws, without introducing dimensional scales. The success (Fig. 2) of this formula implies that blastwave shocks are controlled primarily by these scalings, even in situations where the postshock flow is quite complicated, including, at times, reverse shocks. This is very convenient, because it allows an accurate estimation of the entropy distribution deposited by this forward shock (although the entropy from a reverse shock is not accounted for). An accurate prediction of the shock velocity and its dependence on the stellar structure also permits a systematic analysis of the dynamics of the high-velocity ejecta (§ 5), including the maximum velocity achieved by the ejecta (§ 5.3) and an analysis of the burst of radiation that occurs at shock breakout (§ 5.3.3).

We find in § 5.3.2 that a star must be sufficiently compact in order to produce any relativistic ejecta; for such stars, we make a rough estimate of the rest mass of relativistic ejecta. Applying these considerations to SN 1998bw and the gamma-ray burst, GRB 9804025, that may be associated with it (Soffita et al. 1998), we find that an explosion of relatively small ejected masses (1 $M_\odot$) and large energy ($\gtrsim 10^{52}$ ergs) could provide enough energy in relativistic ejecta both for the gamma-ray burst (Galama et al. 1998) and to power the inferred relativistically expanding synchrotron shell (Kulkarni et al. 1998). Woosley et al. (1998) considered models for SN 1998bw with larger ejected masses in order to fit the supernova light curve, and found accordingly smaller energies in the relativistic ejecta. Even assuming the existence of this ejecta, liberating its energy in a brief period requires an unusually high circumstellar density, as Woosley et al. point out.

The velocity at which stellar material expands into space is related to the velocity of the shock front that set it into motion. However, the nature of this relationship is very different for material deep in the ejected envelope than for material near the stellar surface. Simple considerations (§ 5) reveal that the highest velocity (initially outermost) material is cast away at some multiple of the shock velocity that traversed it, although the value of this factor varies with initial depth. At lower velocities, the smoothness of the pressure distribution controls the density distribution of the ejecta from deep within the progenitor. Here the shock velocity determines the final velocity indirectly, by means of the entropy distribution. The transition between these two behaviors is the result of a complicated, spherical rarefaction flow, but simple models for the pressure distribution (§ 6) reproduce this transition quite accurately, especially in polytropic progenitors for which the high-velocity behavior is well understood (§ 5.2). Features in the ejecta at low velocities, most notably the structure of the ejected mantle, can be understood on the basis of approximate pressure equilibrium.

One consequence of pressure equilibrium for the low-velocity ejecta is the presence a sharp density jump at the base of the outer envelope: the helium ejecta is denser and has a lower entropy than the hydrogen ejecta that surrounds it. This jump, quantified in § 6.1, is greater in the ejecta from red supergiants (about a factor of 30) than from blue supergiants (about a factor of three). It results directly from the density difference between envelopes in a progenitor and the shock acceleration that occurs there. As we have discussed, this feature is unlikely to be affected by the development of reverse shocks or the Rayleigh-Taylor instability and may have interesting observational implications in the epoch of recombination.

The much larger drop in density from helium to hydrogen between red and blue supergiants also leads to a much stronger reverse shock in RSGs than in BSGs. This limits the accuracy of our pressure-based models, which do not include the entropy deposited in the helium mantles (particularly in RSG mantles) by the reverse shock. It also has important consequences for the velocity of radioactive material in the ejecta. Consider, for instance, the fate of the innermost 0.5 $M_\odot$ of ejecta in the 15 $M_\odot$ RSG and the 16 $M_\odot$ BSG progenitors depicted in Figures 7 and 8. In the numerical simulations, which include reverse shocks, this 0.5 $M_\odot$ is 1–3 times more dense at a given time in the RSG ejecta than in the BSG ejecta (the comparison is straightforward, since the ejected masses are quite similar). Because the outer envelope harbors almost all of the energy in the final state, its expansion velocity is essentially fixed, so the expansion velocity of the mantle is determined by its density relative to the outer envelope, which depends on the difference in entropy between the two regions. This, in turn, is affected by the reverse shock. Our pressure-based models indicate what might happen if the reverse shock never developed and the mantle were decelerated by a compression wave instead: it would then lack the reverse shock entropy and be much denser (and expand more slowly) in comparison to the outer envelope. Although these concepts are the products of spherically symmetric models, similar considerations should apply in realistic explosions as well.

It is noteworthy that the reverse shock develops inward (in mass) from the density jump between the helium and hydrogen ejecta, so that there is a density peak at the outer helium ejecta in red supergiants (Fig. 7).

In BSGs the reverse shock is much less severe than for RSGs, and (at least for the model 16 $M_\odot$ BSG provided by Nomoto) seems to develop far inward in mass from the hydrogen-helium boundary. The pressure-based model tracks the mantle ejecta quite well. Indeed, the difference between the mantle and the outer envelope can be ignored entirely without too much error: such is the spirit of the Chevalier & Soker (1989) model for SN 1987A, whose elements we have incorporated into our harmonic-mean model for BSGs. Here, the mantle and the inner region of the hydrogen ejecta can be grouped together as a single region of gently declining density.

Regardless of the mantle, it appears that the ejecta density distribution in the bulk of the hydrogen envelope is a flat or gently declining function of velocity (or mass) for both red and blue supergiants. At some break velocity, the structure of $\rho_f(v_f)$ rolls over toward the steeply declining

power law it must assume at high velocities. For red supergiants, a quantitative statement can be made: density falls by only 20%–40% in the inner one-half of the hydrogen ejecta mass. (This density drop decreases with increasing mass ratio q, despite the fact that the inner power law l_1 gets steeper [Table 4], but note that the hydrogen envelope is a smaller fraction of the ejecta as q increases.)

Chevalier (1976), making an analogy with Sedov blastwaves of different indices, suggested that a detached shell (density maximum) should form in the ejecta at shells for which $d \ln \rho_0 / d \ln r_0$ decreases smoothly through the value -2.53 in the progenitor. If this were strictly true, a detached shell would form in the outer envelope ejecta of all the progenitors we have considered. No such density maxima actually formed in the outer envelopes, although density maxima did occur in the ejected mantles (of RSGs especially, as described above). The presence of density maxima in the ejected mantles depends on the strength of the reverse shock and does not appear to be related to Chevalier's proposed mechanism.

It is clear from our simulations that when a progenitor deviates from a polytropic structure in the outer one-half of its radius, perhaps because of inefficient convection or the details of radiative transfer, the resulting high-velocity ejecta distribution bears the imprint of this effect. This is apparent when the ejecta from simulations with realistic stellar progenitors are compared against the ejecta of polytropic models. Our analysis of the high-velocity ejecta of polytropic models is limited in applicability by this effect. On the other hand, the relative constancy of the shock-velocity parameter β_1, the postshock acceleration ratio $(v_f/v_s)_p$, and the truncation radius R_t for planar acceleration all suggest that it may be possible to extend our semi-analytical theory to accommodate variations in $n_{\rm eff}$. With such a theory, it may even be possible to constrain models of inefficient convection with the early light curves of Type II supernovae.

Our pressure-based model, being derived from a simple model for the entropy deposited in the blastwave shock, is a local theory that relates the final density ρ_f of a mass shell with its initial density ρ_0, initial radius r_0, and enclosed ejected mass m. A strong reverse shock, whose passage cannot be predicted by these local variables alone, invalidates this model in the mantles of stars. But, the local theory is exceptionally accurate where it is valid.

Our harmonic-mean models, on the other hand, are global models for the ejecta distributions of supernovae, in the sense that they specify the general run of final density versus velocity that results from a specific type of progenitor structure. These models are appealing for their simplicity, although they contain little information about the dynamics of envelope expulsion in supernovae.

The authors are indebted to Stan Woosley and Ken'ichi Nomoto for providing supernova progenitor structures, and to J. Kelly Truelove for providing the computer code that we modified for the purposes of this paper. C. D. M. thanks John Monnier, Ben Metcalf, and George McLean for many valuable suggestions, Lars Bildsten for clarifying stellar structure and evolution and reviewing a draft of this work, and Douglas Leonard for discussing light curves. We also wish to thank our referee, Roger Chevalier, for insightful and helpful comments. C. D. M. was supported in part by a National Science Foundation Graduate Fellowship and an ARCS fellowship. The research of both C. D. M. and C. F. M. is supported in part by the National Science Foundation through NSF grant AST 95-30480.

APPENDIX

FULLY LAGRANGIAN, SELF-SIMILAR TREATMENT OF SHOCK EMERGENCE

We present a calculation of the self-similar, planar flow in a power-law density distribution with an edge, the problem posed by Gandel'man & Frank-Kamenetsky (1956) and solved by Sakurai (1960). Unlike previous treatments, we use a Lagrangian approach for the prebreakout flow as well as the postbreakout flow. This has the advantage that variables can be compared against their postshock values, rather than against their breakout values (which previously were related to postshock values with an Eulerian treatment). To do this, we first define the space and time coordinates $x \equiv 1 - r/R_*$ and $\Delta t \equiv t - t(\text{breakout})$. The time at which a mass shell experiences the shock is $\Delta t_0(m)$. For our self-similar coordinate we choose $\eta \equiv \Delta t/\Delta t_0(m)$, and for the flow variable we choose $S(\eta) = x(m)/x_0(m)$. Our variables η and $S(\eta)$ are both unity in the initial state, and decrease toward $-\infty$ as the flow progresses. Breakout occurs when $\Delta t = \eta = 0$.

To maintain consistency with previous authors, we define the initial density distribution as $\rho_0(m) = k_1[R_* x_0(m)]^n$ and the shock velocity to be $v_s = -k_2[R_* x_0(m)]^{-\lambda}$, where $\lambda \equiv n\beta_1$. Then, $\Delta t_0 = -(R_* x_0)^{1-\lambda}/k_2(1+\lambda)$.

Considering the time variable Δt to be parameterized by η and x_0, the constraint of constant time, $d\Delta t = 0$, gives $d\eta = -\eta(1-\lambda)dx_0/x_0$. This relation allows us to take the necessary derivatives to solve for the flow. First of these is the density, defined in planar geometry by

$$\rho(\eta, x_0) = \rho_0 \left(\frac{dx_0}{dx} \right)_{\Delta t} = \frac{\rho_0}{S(\eta) - (\lambda+1)\eta S'(\eta)} . \tag{A1}$$

Now, we evaluate the pressure as $p(\eta, x_0) = p_s(\rho/\rho_s)^\gamma$, where p_s and ρ_s are the postshock pressure and density. The acceleration in planar geometry is $R_* \ddot{x} = -(dp/dr)_{\Delta t}/\rho = -(dp/dr_0)_{\Delta t}/\rho_0$. From the definitions of $S(\eta)$ and η, on the other hand, $\ddot{x} = x_0 S''(\eta)/t_0^2$. Combining the two expressions for the acceleration, we have the following differential equation for $S(\eta)$ to describe planar, self-similar flow:

$$(1+\lambda)^2 S'' = -\frac{2}{\gamma+1}\left(\frac{\gamma-1}{\gamma+1}\right)^\gamma \left\{ \frac{n-2\lambda}{[S-(\lambda+1)\eta S']^\gamma} - \gamma(\lambda-1)\eta \frac{\lambda S' + (\lambda-1)\eta S''}{[S-(\lambda+1)\eta S']^{\gamma+1}} \right\} . \tag{A2}$$

The initial condition for this equation is at the time $\eta = 1$, when a mass shell is hit by the shock wave. Because the mass shell is in its initial position at this time, and because its postshock density and velocity are given by the Rankine-Hugoniot jump conditions for strong shocks,

$$S(1) = 1\ , \qquad S'(1) = \frac{2}{(\gamma + 1)(\lambda + 1)}\ . \tag{A3}$$

Note that the ratio v/v_s at any point in the flow is equal to $(\lambda + 1)S'(\eta)$, for the value of η appropriate to the time and mass shell considered.

We used the technique described by Sakurai to determine λ (or equivalently β_1) for $\gamma = 4/3$ and $n = 3/2$ and 3. Then we solved for the evolution of a mass shell's position using equation (A2), starting with the initial conditions of equation (A3). We continued the numerical solution out to $|\eta| > 10^8$ and used the known asymptotic solution to find the limit $S'(\eta \to -\infty)$. For the purpose of studying the solution, we then fit the resulting velocity history v/v_s in powers of $(2 - \eta)^{-1/3}$. This parameterization was chosen to show the asymptotic dependence of $S(\eta)$ as $\eta \to -\infty$, and also to be finite for all $\eta < 1$. We obtain

$$\frac{v(m, \eta)}{v_s(m)} \simeq 2.1649 - \frac{1.0656}{(2 - \eta)^{1/3}} + \frac{0.5872}{(2 - \eta)^{2/3}} - \frac{1.1235}{2 - \eta} \qquad \left(n = \frac{3}{2}\right),$$

$$\frac{v(m, \eta)}{v_s(m)} \simeq 2.0351 - \frac{0.7638}{(2 - \eta)^{1/3}} + \frac{0.2535}{(2 - \eta)^{2/3}} - \frac{0.7861}{2 - \eta} \qquad (n = 3)\ . \tag{A4}$$

These fits, meant to capture the late-time evolution accurately, are accurate to within 2% and 1.5%, respectively, for $\eta < -1$, although they miss the breakout value ($v_f/v_s = 6/7$) by 34% and 14%, respectively. For the purpose of studying the truncation of the self-similar acceleration law, as discussed in § 5, it is useful to make similar fits based on the normalized distance coordinate $S(\eta) = x/x_0$ rather than the time coordinate η:

$$\frac{v(m, S)}{v_s(m)} \simeq 2.1649 - \frac{1.2504}{(2 - S)^{1/3}} + \frac{0.8473}{(2 - S)^{2/3}} - \frac{0.9817}{2 - S} \qquad \left(n = \frac{3}{2}\right),$$

$$\frac{v(m, S)}{v_s(m)} \simeq 2.0351 - \frac{0.8260}{(2 - S)^{1/3}} + \frac{0.3094}{(2 - S)^{2/3}} - \frac{0.5244}{2 - S} \qquad (n = 3)\ . \tag{A5}$$

Much like the previous fits, these are both valid to within 1% for $S < -1$, but they miss the breakout value by 9% and 16%, respectively.

Litvinova & Nadëzhin (1990) suggested that spherical effects would act to truncate the planar acceleration once a shell had reached a truncation radius $R_t \gtrsim R_*$. Using our solution to the self-similar expansion, we can evaluate this prescription for different truncation radii and compare it to the results of fully spherical calculations (§ 5.2). The normalized position S_t corresponding to R_t is

$$S_t = -\frac{R_t/R_* - 1}{x_0}\ . \tag{A6}$$

Taking $R_t = 3\ R_*$ as an illustrative example (Fig. 3), the self-similar solution can be fit as a polynomial in $x_0^{1/3}$ in accordance with equation (A6):

$$\frac{v_f(r_0)}{v_s(r_0)} \simeq \left(\frac{v_f}{v_s}\right)_p (1 - 0.4522x_0^{1/3} + 0.1717x_0^{2/3} - 0.04328x_0) \qquad \left(n = \frac{3}{2}\right),$$

$$\frac{v_f(r_0)}{v_s(r_0)} \simeq \left(\frac{v_f}{v_s}\right)_p (1 - 0.3174x_0^{1/3} + 0.0373x_0^{2/3} + 0.0199x_0) \qquad (n = 3)\ . \tag{A7}$$

These fit the self-similar solution quite well, with maximum errors of 0.3% and 0.5% for $n = 3/2$ and 3, respectively, in the entire range $0 < x_0 < 1$. Clearly these are quite similar to the outcome of full spherical dynamics as given by equation (26).

REFERENCES

Arnett, D. 1997, Supernovae and Nucleosynthesis (New York: Princeton Univ. Press)
Arnett, D., Fryxell, B., & Müller, E. 1989, ApJ, 341, L63
Bethe, H. A., & Pizzochero, P. 1990, ApJ, 350, L33
Chandrasekhar, S. 1939, An Introduction to the Theory of Stellar Structure (New York: Dover)
Chevalier, R. A. 1976, ApJ, 207, 872
———. 1982, ApJ, 258, 790
———. 1990, ApJ, 359, 463
———. 1992, ApJ, 394, 599
Chevalier, R. A., & Klein, R. I. 1979, ApJ, 234, 597
Chevalier, R. A., & Soker, N. 1989, ApJ, 341, 867
Colgate, S. A. 1995, Phys. Rep., 256, 1
Colgate, S. A., & Johnson, M. H. 1960, Phys. Rev. D, 5, 235
Colgate, S. A., & White, R. H. 1966, ApJ, 143, 626
Dwarkadas, V. V., & Chevalier, R. A. 1998, ApJ, submitted
Eastman, R. G., Schmidt, B. P., & Kirshner, R. 1996, ApJ, 466, 911
Ensman, L., & Burrows, A. 1992, ApJ, 393, 742
Falk, S. W., & Arnett, W. D. 1977, ApJ, 33, 515
Filippenko, A. V. 1997, ARA&A, 35, 309
Fransson, C., Lundqvist, P., & Chevalier, R. A. 1996, ApJ, 461, 993
Galama, T. J. et al. 1998, Nature, submitted
Gandel' man, G. M., & Frank-Kamenetsky, D. A. 1956, Soviet Phys. Dokl., 1, 223
Heger, A., Jeannin, L., Langer, N., & Baraffe, I. 1997, A&A, 327, 224
Herant, M., & Woosley, S. E. 1994, ApJ, 425, 814
Imshennik, V. S., & Nadëzhin, D. K. 1989, Soviet Sci. Rev. E. Astrophys Space Phys., 8, 1
Johnson, M. H., & McKee, C. F. 1971, Phys. Rev. D, 3, 858
Kazhdan, Y. M., & Murzina, M. 1992, ApJ, 400, 192

Klein, R. I., & Chevalier, R. A. 1978, ApJ, 223, L109
Klimishin, I. A., & Gnatyk, B. I. 1982, Astrophysics, 17, 306
Kompaneets, A. S. 1960, Soviet Phys. Dokl., 5, 46
Koo, B.-C., & McKee, C. F. 1990, ApJ, 354, 513
Kulkarni, S. R., et al. 1998, Nature, submitted
Laumbach, D. D., & Probstein, R. F. 1969, J. Fluid Mech., 35, 53
Li, H., McCray, R., & Sunyaev, R. 1993, ApJ, 419, 824
Litvinova, I. Y., & Nadëzhin, D. K. 1990, Soviet Astron. Lett., 16, 29
Luo, D., & Chevalier, R. A. 1994, ApJ, 435, 815
Maeder, A. 1992, A&A, 264, 105
McCray, R. 1993, ARA&A, 31,175
McKee, C. F. 1974, ApJ, 188, 335
Nomoto, K., Iwamoto, K., & Suzuki, T. 1995, Phys. Rep., 256, 173
Nomoto, K., & Sugimoto, D. 1972, Prog. Theor. Phys., 48, 1972
Ostriker, J. P., & McKee, C. F. 1988, Rev. Mod. Phys., 60, 1
Richtmyer, R. D., & Morton, K. W. 1967, Difference Methods for Initial-Value Problems (New York: Interscience)
Sakurai, A. 1960, Comm. Pure Appl. Math., 13, 353
Sedov, L. I. 1959, Similarity and Dimensional Methods in Mechanics (New York: Academic)
Shigeyama, T., & Nomoto, K. 1990, ApJ, 360, 242
Shigeyama, T., Suzuki, T., Kumagai, S., Nomoto, K., Saio, H., & Yamaoka, H. 1994, ApJ, 420, 341
Soffita, P. et al. 1998, IAU Circ. 6884
Suzuki, T., & Nomoto, K. 1995, ApJ, 455, 658
Taylor, G. I. 1950, Proc. R. Soc. London A, 201, 175
Truelove, J. K., & McKee, C. F. 1998, ApJ, submitted
Weaver, T. A. 1976, ApJS, 32, 233
Whitham, G. B. 1974, Linear and Nonlinear Waves (New York: Wiley)
Woosley, S. E., Eastman, R. G., & Schmidt, B. P. 1998, ApJ, submitted
Woosley, S. E., Langer, N., & Weaver, T. A. 1993, ApJ, 411, 823
———. 1995, ApJ, 448, 315
Woosley, S. E., & Weaver, T. A. 1995, ApJS, 101, 181